The Report Committee for Saumik P. Dana certifies that this is the approved version of the following report

Simulation of growth of multiple interacting 3D Cracks in hydraulic fractures driven by inviscid fluid

APPROVED BY

SUPERVISING COMMITTEE:

Mark E. Mear, Supervisor

Gregory J. Rodin

Simulation of growth of multiple interacting 3D Cracks in hydraulic fractures driven by inviscid fluid

by

Saumik P. Dana, B.E.;M.E.

REPORT

Presented to the Faculty of the Graduate School of

The University of Texas at Austin

in Partial Fulfillment

of the Requirements

for the Degree of

MASTER OF SCIENCE IN ENGINEERING

THE UNIVERSITY OF TEXAS AT AUSTIN

December 2014

Acknowledgments

I wish to thank my advisor Prof. Mark E. Mear for his guidance and support over the course of this endeavor. I would like to thank Dr. Rick Dean and Dr. Joseph Schmidt of Conoco-Phillips for their financial support and technical guidance during the course of this investigation. Finally, I would like to thank my family and friends for their love and support.

Simulation of growth of multiple interacting 3D Cracks in hydraulic fractures driven by inviscid fluid

Saumik P. Dana, M.S.E.
The University of Texas at Austin, 2014

Supervisor: Mark E. Mear

In this report, we develop a computational procedure to investigate propagation of 3D cracks in isotropic linearly elastic media in a 2D framework. We reduce the 3D weakly singular, weak-form traction integral equation to its 2D analog by introducing a constraint on crack profile in out-of-plane direction. Symmetric Galerkin boundary element method based on the obtained 2D weak-form traction integral equation is adopted to model these fractures. In particular, we consider multiple interacting cracks in unbounded domain subject to internal pressure to model hydraulic fracture.

Table of Contents

List of Figures

Chapter 1

Introduction

In this report a computational procedure is developed to investigate effect of crack height and cross section profile on crack propagation in isotropic linearly elastic unbounded media subject to internal pressure. We first present the computational procedure and solution strategy utilized in our boundary element method code which we will call HyFrac2D. We verify the accuracy of our numerical technique and study effect of crack height and cross section profile on SIF at crack tip, fracture pressure and fracture volume for a single crack subject to internal pressure. We then study effect of crack height and cross section profile on crack growth for two aligned cracks and three aligned cracks with equal injection pressures. We then do a comparison between crack growth for multiply aligned cracks subject to equal injection pressures and equal injection volumes.

Chapter 2

Computational Procedure and Solution Strategy

2.1 Governing Equation for Fracture

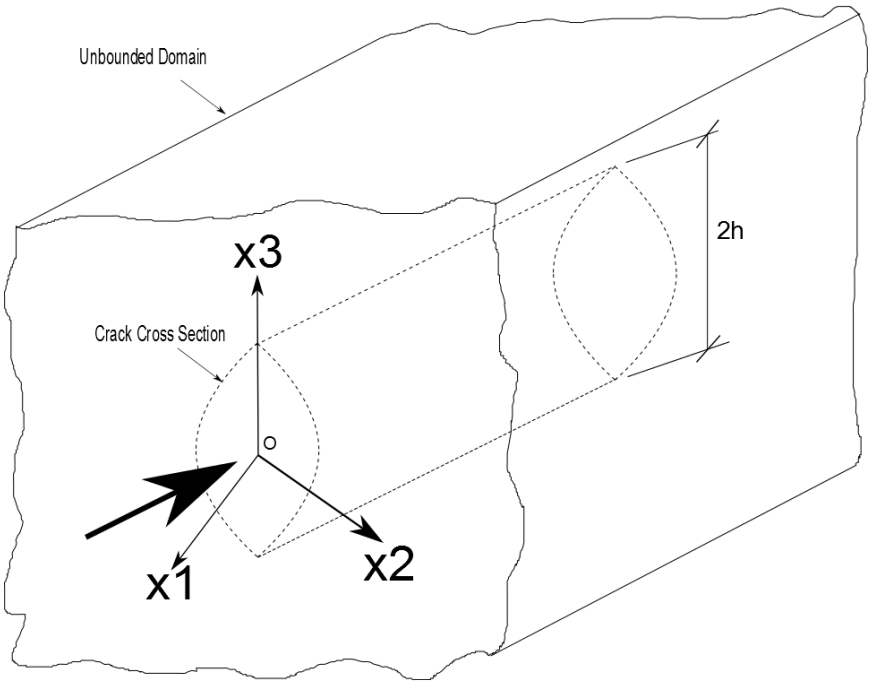

Figure 2.1: Schematic for 3D crack of size $2h$ and constraint imposed on cross section in z direction. The crack resides in an isotropic linearly elastic unbounded domain. This assumed geometry is typical of hydraulic fractures. The thick arrow pointing towards O shows the view with respect to which the cross section profile is given in Figure 2.2.

Figure 2.1 shows assumed geometry of cracks. Figure 2.2 shows the cross section for different constraints.

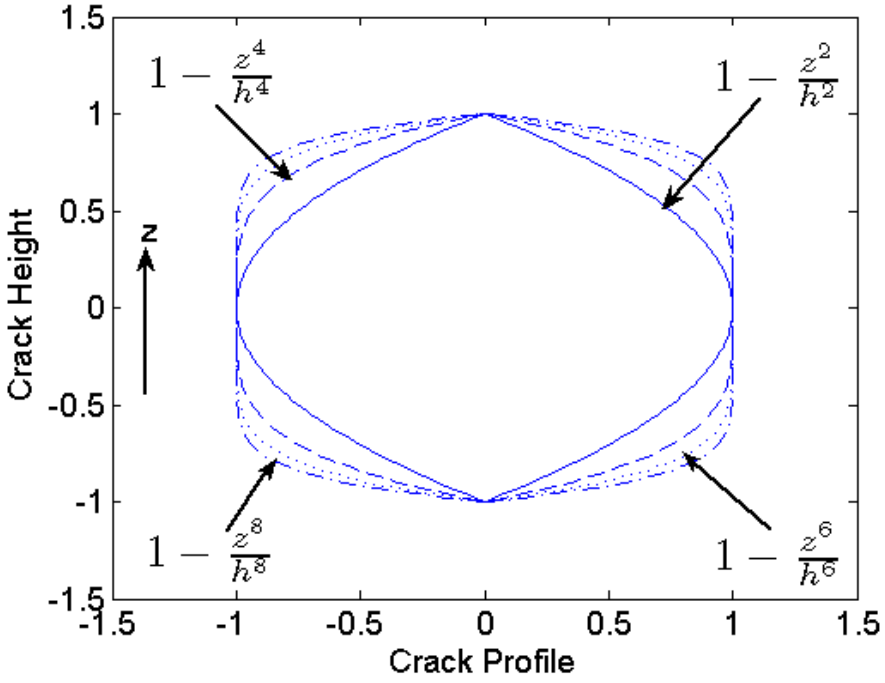

Figure 2.2: Cross sections for $(1-\frac{z^2}{h^2})$, $(1-\frac{z^4}{h^4})$, $(1-\frac{z^6}{h^6})$ and $(1-\frac{z^8}{h^8})$ profiles.

The 3D weak-form traction integral equation for cracks in unbounded domain is [1]

$$-\int_\Gamma t_\alpha(\boldsymbol{x})\Delta\tilde{u}^o_\alpha(\boldsymbol{x})d\Gamma(\boldsymbol{x})$$

$$=\int_\Gamma\int_\Gamma D_t(\boldsymbol{x})\Delta\tilde{u}^o_\alpha(\boldsymbol{x})C^{t\alpha}_{m\beta}(\boldsymbol{\xi}-\boldsymbol{x})D_m(\boldsymbol{\xi})\Delta u^o_\beta(\boldsymbol{\xi})d\Gamma(\boldsymbol{\xi})d\Gamma(\boldsymbol{x}) \tag{2.1}$$

where $\boldsymbol{x}\equiv\{x_1,x_2,x_3\}$ is the *source point*, $\boldsymbol{\xi}\equiv\{\xi_1,\xi_2,\xi_3\}$ is *field point*, $t_\alpha(\boldsymbol{x})$ is the traction on crack as a function $\boldsymbol{x}$, $\Delta\tilde{u}^o_\alpha(\boldsymbol{x})$ is crack displacement test field as a function of $\boldsymbol{x}$, $D_t(\boldsymbol{x})$ and $D_m(\boldsymbol{\xi})$ are surface differentials, $\Delta u^o_\beta(\boldsymbol{\xi})$ is

the actual crack displacement field, $C^{t\alpha}_{m\beta}(\boldsymbol{\xi}-\boldsymbol{x})$ is a weakly singular kernel, Γ is crack surface and $\alpha,\beta=1,2$. The constraint on crack profile is introduced as a constraint on the crack displacement field as a function of $\boldsymbol{x}$ as follows

$$\Delta\tilde{u}^o_\alpha(x_1,x_2,x_3)=F(x_3,h)\times\Delta\tilde{u}_\alpha(x_1,x_2)$$

where $\Delta\tilde{u}_\alpha(x_1,x_2)$ is the 2D analog of crack displacement field $\Delta\tilde{u}^o_\alpha(x_1,x_2,x_3)$. The same idea applies to crack displacement field as a function of $\boldsymbol{\xi}$ as follows

$$\Delta\tilde{u}^o_\alpha(\xi_1,\xi_2,\xi_3)=F(\xi_3,h)\times\Delta\tilde{u}_\alpha(\xi_1,\xi_2)$$

2.1.1 $F(x_3,h)=1-\frac{x_3^2}{h^2}$ and $F(\xi_3,h)=1-\frac{\xi_3^2}{h^2}$

We introduce the following constraint on crack profile in x_3 and ξ_3 directions

$$\Delta\tilde{u}^o_\alpha(x_1,x_2,x_3)=(1-\frac{x_3^2}{h^2})\Delta\tilde{u}_\alpha(x_1,x_2) \tag{2.2}$$

$$\Delta u^o_\beta(\xi_1,\xi_2,\xi_3)=(1-\frac{\xi_3^2}{h^2})\Delta u_\beta(\xi_1,\xi_2) \tag{2.3}$$

The surface differentials $D_m(\boldsymbol{\xi})$ are

$$D_m(\boldsymbol{\xi})\equiv n_i\epsilon_{ikm}\frac{\partial}{\partial\xi_k}=n_1\epsilon_{1km}\frac{\partial}{\partial\xi_k}+n_2\epsilon_{2km}\frac{\partial}{\partial\xi_k}$$

$$=n_1(\boldsymbol{\xi})\epsilon_{12m}\frac{\partial}{\partial\xi_2}+n_1(\boldsymbol{\xi})\epsilon_{13m}\frac{\partial}{\partial\xi_3}+n_2(\boldsymbol{\xi})\epsilon_{21m}\frac{\partial}{\partial\xi_1}+n_2(\boldsymbol{\xi})\epsilon_{23m}\frac{\partial}{\partial\xi_3}$$

$$=(n_1(\boldsymbol{\xi})\epsilon_{13m}+n_2(\boldsymbol{\xi})\epsilon_{23m})\frac{\partial}{\partial\xi_3}+n_1(\boldsymbol{\xi})\epsilon_{12m}\frac{\partial}{\partial\xi_2}+n_2(\boldsymbol{\xi})\epsilon_{21m}\frac{\partial}{\partial\xi_1}$$

Substituting m=1,2,3 sucessively, we get[1]

$$D_1(\boldsymbol{\xi})\equiv n_2(\boldsymbol{\xi})\frac{\partial}{\partial\xi_3}$$

[1] $n_1=\frac{d\xi_2}{ds}\quad|\quad n_2=-\frac{d\xi_1}{ds}$

$$D_2(\boldsymbol{\xi}) \equiv -n_1(\boldsymbol{\xi})\frac{\partial}{\partial \xi_3}$$

$$D_3(\boldsymbol{\xi}) \equiv n_1(\boldsymbol{\xi})\frac{\partial}{\partial \xi_2} - n_2(\boldsymbol{\xi})\frac{\partial}{\partial \xi_1} \equiv \frac{\partial}{\partial s}$$

Applying the obtained differentials on the constraint function in $\boldsymbol{\xi}$

$$D_1(\boldsymbol{\xi})(1 - \frac{\xi_3^2}{h^2}) = -n_2(\boldsymbol{\xi})\frac{2\xi_3}{h^2}$$

$$D_2(\boldsymbol{\xi})(1 - \frac{\xi_3^2}{h^2}) = n_1(\boldsymbol{\xi})\frac{2\xi_3}{h^2}$$

$$D_3(\boldsymbol{\xi})(1 - \frac{\xi_3^2}{h^2}) = (1 - \frac{\xi_3^2}{h^2})\frac{\partial}{\partial s}$$

Similarly, applying $D_t(\boldsymbol{x})$ on constraint function in $\boldsymbol{x}$

$$D_1(\boldsymbol{x})(1 - \frac{x_3^2}{h^2}) = -n_2(\boldsymbol{x})\frac{2x_3}{h^2}$$

$$D_2(\boldsymbol{x})(1 - \frac{x_3^2}{h^2}) = n_1(\boldsymbol{x})\frac{2x_3}{h^2}$$

$$D_3(\boldsymbol{x})(1 - \frac{x_3^2}{h^2}) = (1 - \frac{x_3^2}{h^2})\frac{\partial}{\partial s}$$

We work on LHS of Eq.(2.1) by incorporating Eq.(2.2)

$$-\int_\Gamma t_\alpha(\boldsymbol{x})\Big\{\int_{-h}^{h}(1 - \frac{x_3^2}{h^2})dx_3\Big\}\Delta\tilde{u}_\alpha(\boldsymbol{x})d\Gamma(\boldsymbol{x}) = -\frac{4h}{3}\int_\Gamma t_\alpha(\boldsymbol{x})\Delta\tilde{u}_\alpha(\boldsymbol{x})d\Gamma(\boldsymbol{x}) \tag{2.4}$$

where now $\boldsymbol{x} \equiv \{x_1, x_2\}$ and $\boldsymbol{\xi} \equiv \{\xi_1, \xi_2\}$. We work on RHS of Eq.(2.1) by incorporating Eqns.(2.2) and (2.3)

$$\int_\Gamma\int_\Gamma\Big\{\int_{-h}^{h} D_t(\boldsymbol{x})(1 - \frac{x_3^2}{h^2})\Delta\tilde{u}_\alpha(\boldsymbol{x})\times$$

$$\Big\{\int_{-h}^{h} C^{t\alpha}_{m\beta}(\boldsymbol{\xi} - \boldsymbol{x})D_m(\boldsymbol{\xi})(1 - \frac{\xi_3^2}{h^2})\Delta u_\beta(\boldsymbol{\xi})d\xi_3\Big\}dx_3\Big\}d\Gamma(\boldsymbol{\xi})d\Gamma(\boldsymbol{x}) \tag{2.5}$$

where now $\boldsymbol{x} \equiv \{x_1, x_2\}$ and $\boldsymbol{\xi} \equiv \{\xi_1, \xi_2\}$. For the purpose of convenience

$$\frac{\mu}{4\pi(1-\nu)} = k(say) = \frac{E}{8\pi(1-\nu^2)}$$

where μ, ν and E are shear modulus, Poisson's ratio and Young's modulus of elastic solid respectively. The closed form expression for $C^{t\alpha}_{m\beta}$ in isotropic solid [1] can be written as

$$C^{t\alpha}_{m\beta} = k[\frac{E^{t\alpha}_{m\beta}}{r} + \frac{F^{t\alpha}_{m\beta}}{r} + \frac{G^{t\alpha}_{m\beta}}{r^3}]$$

where $E^{t\alpha}_{m\beta}$, $F^{t\alpha}_{m\beta}$ and $G^{t\alpha}_{m\beta}$ are given as

$$E^{t\alpha}_{m\beta} \equiv (1-\nu)\delta_{t\alpha}\delta_{m\beta} + 2\nu\delta_{m\alpha}\delta_{t\beta}$$

$$F^{t\alpha}_{m\beta} \equiv -\delta_{\alpha\beta}\delta_{tm}$$

$$G^{t\alpha}_{m\beta} \equiv -\delta_{tm}r_\beta r_\alpha$$

r is distance between source and field point in 3D framework

$$r = \sqrt{(\xi_1 - x_1)^2 + (\xi_2 - x_2)^2 + (\xi_3 - x_3)^2}$$

ρ is distance between source and field point in 2D framework

$$\rho = \sqrt{(\xi_1 - x_1)^2 + (\xi_2 - x_2)^2}$$

r and ρ are related by

$$r = \sqrt{\rho^2 + (\xi_3 - x_3)^2}$$

We first evaluate term inside inner brace brackets of expression (2.5)

$$\int_{-h}^{h} C^{t\alpha}_{m\beta} D_m(\boldsymbol{\xi})(1 - \frac{\xi_3^2}{h^2})\Delta u_\beta(\boldsymbol{\xi}) d\xi_3$$

$$= \int_{-h}^{h} k[\frac{E_{m\beta}^{t\alpha}}{r} + \frac{F_{m\beta}^{t\alpha}}{r} + \frac{G_{m\beta}^{t\alpha}}{r^3}]D_m(\boldsymbol{\xi})(1 - \frac{\xi_3^2}{h^2})\Delta u_\beta(\boldsymbol{\xi})d\xi_3 \tag{2.6}$$

For the purpose of convenience, we use the following

$$f_1 = \int_{-h}^{h} \frac{\xi_3}{r} d\xi_3$$

$$f_2 = \int_{-h}^{h} (\frac{h^2}{r^3} - \frac{\xi_3^2}{r^3}) d\xi_3$$

$$f_3 = \int_{-h}^{h} (\frac{h^2}{r} - \frac{\xi_3^2}{r}) d\xi_3$$

$$f_4 = \int_{-h}^{h} \frac{\xi_3}{r^3} d\xi_3$$

And the following

$$E^t(\boldsymbol{\xi}) = \frac{2k\Delta u_\beta}{h^2}(E_{2\beta}^{t\alpha} n_1(\boldsymbol{\xi}) - E_{1\beta}^{t\alpha} n_2(\boldsymbol{\xi}))$$

$$F^t(\boldsymbol{\xi}) = \frac{2k\Delta u_\beta(\boldsymbol{\xi})}{h^2}(F_{2\beta}^{t\alpha} n_1(\boldsymbol{\xi}) - F_{1\beta}^{t\alpha} n_2(\boldsymbol{\xi}))$$

$$H^t(\boldsymbol{\xi}) = E^t(\boldsymbol{\xi}) + F^t(\boldsymbol{\xi}) = \frac{2k\Delta u_\beta}{h^2}((E_{2\beta}^{t\alpha} + F_{2\beta}^{t\alpha}) n_1(\boldsymbol{\xi}) - (E_{1\beta}^{t\alpha} + F_{1\beta}^{t\alpha}) n_2(\boldsymbol{\xi}))$$

$$G_1^t(\boldsymbol{\xi}) = \frac{k}{h^2} G_{3\beta}^{t\alpha} D_3 \Delta u_\beta(\boldsymbol{\xi})$$

$$F_1^t(\boldsymbol{\xi}) = \frac{k}{h^2} F_{3\beta}^{t\alpha} D_3 \Delta u_\beta(\boldsymbol{\xi})$$

$$G^t(\boldsymbol{\xi}) = \frac{2k\Delta u_\beta(\boldsymbol{\xi})}{h^2}(G_{2\beta}^{t\alpha} n_1(\boldsymbol{\xi}) - G_{1\beta}^{t\alpha} n_2(\boldsymbol{\xi}))$$

We evaluate first term on RHS of Eq.(2.6)

$$\int_{-h}^{h} k\frac{E_{m\beta}^{t\alpha}}{r} D_m(\boldsymbol{\xi})(1 - \frac{\xi_3^2}{h^2})\Delta u_\beta(\boldsymbol{\xi})d\xi_3 = E^t(\boldsymbol{\xi}) f_1 \tag{2.7}$$

We evaluate second term on RHS of Eq.(2.6)

$$\int_{-h}^{h} k\frac{F_{m\beta}^{t\alpha}}{r} D_m(\boldsymbol{\xi})(1 - \frac{\xi_3^2}{h^2})\Delta u_\beta(\boldsymbol{\xi})d\xi_3 = F^t(\boldsymbol{\xi}) f_1 + F_1^t(\boldsymbol{\xi}) f_3 \tag{2.8}$$

We evaluate third term on RHS of Eq.(2.6)

$$\int_{-h}^{h} k\frac{G^{t\alpha}_{m\beta}}{r^3}D_m(\boldsymbol{\xi})(1-\frac{\xi_3^2}{h^2})\Delta u_\beta(\boldsymbol{\xi})d\xi_3 = G^t(\boldsymbol{\xi})f_4 + G^t_1(\boldsymbol{\xi})f_2 \tag{2.9}$$

We substitute Eqns.(2.7),(2.8) and (2.9) in Eq.(2.6) to obtain

$$\int_{-h}^{h} C^{t\alpha}_{m\beta}D_m(\boldsymbol{\xi})(1-\frac{\xi_3^2}{h^2})\Delta u_\beta(\boldsymbol{\xi})d\xi_3 = H^t(\boldsymbol{\xi})f_1 + G^t_1(\boldsymbol{\xi})f_2 + F^t_1(\boldsymbol{\xi})f_3 + G^t(\boldsymbol{\xi})f_4 \tag{2.10}$$

We use Eq.(2.10) to obtain

$$\int_{-h}^{h} D_t(\boldsymbol{x})(1-\frac{x_3^2}{h^2})\Delta\tilde{u}_\alpha(\boldsymbol{x})\Big\{\int_{-h}^{h} C^{t\alpha}_{m\beta}(\boldsymbol{\xi}-\boldsymbol{x})D_m(\boldsymbol{\xi})(1-\frac{\xi_3^2}{h^2})\Delta u_\beta(\boldsymbol{\xi})d\xi_3\Big\}dx_3$$

$$= \int_{-h}^{h}\sum_{t=1}^{3}\Big(H^t(\boldsymbol{\xi})f_1 + G^t_1(\boldsymbol{\xi})f_2 + F^t_1(\boldsymbol{\xi})f_3 + G^t(\boldsymbol{\xi})f_4\Big)D_t(\boldsymbol{x})(1-\frac{x_3^2}{h^2})\Delta\tilde{u}_\alpha(\boldsymbol{x})dx_3 \tag{2.11}$$

For the purpose of convenience, we use

$$L = ln(\frac{2h+\sqrt{\rho^2+4h^2}}{\rho})$$

$$M = \rho - \sqrt{\rho^2+4h^2}$$

$$N = \sqrt{\rho^2+4h^2}$$

To be able to evaluate RHS of Eq.(2.11), we need to evaluate the following

$$\int_{-h}^{h} x_3 f_1 dx_3 = \frac{4h^3}{3}L + (2h^2+\frac{2\rho^2}{9})M + \frac{4h^2}{9}N = A$$

$$\int_{-h}^{h} x_3 f_4 dx_3 = -\frac{2}{3}(1+\frac{3h^2}{\rho^2})M - \frac{4h^2}{3\rho^2}N = B$$

$$\int_{-h}^{h}(1-\frac{x_3^2}{h^2})f_2 dx_3 = -(\frac{8\rho^2}{45h^2}+\frac{8}{3})M + (\frac{16h^2}{15\rho^2}-\frac{16}{45})N - \frac{8h}{3}L = C$$

$$\int_{-h}^{h}(1-\frac{x_3^2}{h^2})f_3dx_3=(\frac{32h^3}{15}+\frac{4\rho^2h}{3})L+(\frac{8\rho^2}{9}+\frac{8\rho^4}{225h^2})M-N(\frac{992h^2}{900}-\frac{64\rho^2}{900})=D$$

RHS of Eqn.(2.11) is finally evaluated as

$$-\frac{4Ak}{h^4}\Bigg\{n_2(\boldsymbol{x})\Bigg((1-\nu)\delta_{1\alpha}\delta_{2\beta}n_1(\boldsymbol{\xi})+2\nu\delta_{2\alpha}\delta_{1\beta}n_1(\boldsymbol{\xi})-(1+\nu)\delta_{\alpha1}\delta_{\beta1}n_2(\boldsymbol{\xi})+\delta_{\alpha\beta}n_2(\boldsymbol{\xi})\Bigg)$$

$$+n_1(\boldsymbol{x})\Bigg((1-\nu)\delta_{2\alpha}\delta_{1\beta}n_2(\boldsymbol{\xi})+2\nu\delta_{1\alpha}\delta_{2\beta}n_2(\boldsymbol{\xi})-(1+\nu)\delta_{\alpha2}\delta_{\beta2}n_1(\boldsymbol{\xi})+\delta_{\alpha\beta}n_1(\boldsymbol{\xi})\Bigg)\Bigg\}\times$$

$$\Delta u_\beta(\boldsymbol{\xi})\Delta\tilde{u}_\alpha(\boldsymbol{x})-\frac{4Bk}{h^4}\Bigg\{n_2(\boldsymbol{x})n_2(\boldsymbol{\xi})\rho_\beta\rho_\alpha+n_1(\boldsymbol{x})n_1(\boldsymbol{\xi})\rho_\beta\rho_\alpha\Bigg\}\Delta u_\beta(\boldsymbol{\xi})\Delta\tilde{u}_\alpha(\boldsymbol{x})$$

$$-\frac{Ck}{h^2}\rho_\beta\rho_\alpha D_3\Delta u_\beta(\boldsymbol{\xi})D_3\Delta\tilde{u}_\alpha(\boldsymbol{x})$$

$$-\frac{Dk}{h^2}\delta_{\alpha\beta}D_3\Delta u_\beta(\boldsymbol{\xi})D_3\Delta\tilde{u}_\alpha(\boldsymbol{x}) \tag{2.12}$$

For the purpose of convenience, we use

$$\phi_1=n_2(\boldsymbol{x})\Bigg((1-\nu)\delta_{1\alpha}\delta_{2\beta}n_1(\boldsymbol{\xi})+2\nu\delta_{2\alpha}\delta_{1\beta}n_1(\boldsymbol{\xi})-(1+\nu)\delta_{\alpha1}\delta_{\beta1}n_2(\boldsymbol{\xi})+\delta_{\alpha\beta}n_2(\boldsymbol{\xi})\Bigg)$$

$$\phi_2=n_1(\boldsymbol{x})\Bigg((1-\nu)\delta_{2\alpha}\delta_{1\beta}n_2(\boldsymbol{\xi})+2\nu\delta_{1\alpha}\delta_{2\beta}n_2(\boldsymbol{\xi})-(1+\nu)\delta_{\alpha2}\delta_{\beta2}n_1(\boldsymbol{\xi})+\delta_{\alpha\beta}n_1(\boldsymbol{\xi})\Bigg)$$

$$\phi_3=n_2(\boldsymbol{x})n_2(\boldsymbol{\xi})\rho_\beta\rho_\alpha+n_1(\boldsymbol{x})n_1(\boldsymbol{\xi})\rho_\beta\rho_\alpha$$

$$\psi_1=\frac{4Ak}{h^4}\phi_1+\frac{4Ak}{h^4}\phi_2+\frac{4Bk}{h^4}\phi_3 \tag{2.13}$$

$$\psi_2=\frac{Ck}{h^2}\rho_\beta\rho_\alpha+\frac{Dk}{h^2}\delta_{\alpha\beta} \tag{2.14}$$

Expression (2.12) can now be written as

$$-\psi_1\Delta u_\beta(\boldsymbol{\xi})\Delta\tilde{u}_\alpha(\boldsymbol{x})-\psi_2D_3\Delta u_\beta(\boldsymbol{\xi})D_3\Delta\tilde{u}_\alpha(\boldsymbol{x}) \tag{2.15}$$

Substituing expression (2.15) into RHS of Eq.(2.11)

$$\int_{-h}^{h}D_t(\boldsymbol{x})\Delta\tilde{u}_\alpha(\boldsymbol{x})\Bigg\{\int_{-h}^{h}C_{m\beta}^{t\alpha}(\boldsymbol{\xi}-\boldsymbol{x})D_m(\boldsymbol{\xi})\Delta u_\beta(\boldsymbol{\xi})d\xi_3\Bigg\}dx_3$$

$$= -\psi_1 \Delta u_\beta(\boldsymbol{\xi}) \Delta \tilde{u}_\alpha(\boldsymbol{x}) - \psi_2 D_3 \Delta u_\beta(\boldsymbol{\xi}) D_3 \Delta \tilde{u}_\alpha(\boldsymbol{x}) \tag{2.16}$$

Substituting Eq.(2.16) into expression (2.5), we get following expression

$$-\int_\Gamma \int_\Gamma \Big\{ \psi_1 \Delta u_\beta(\boldsymbol{\xi}) \Delta \tilde{u}_\alpha(\boldsymbol{x}) + \psi_2 D_3 \Delta u_\beta(\boldsymbol{\xi}) D_3 \Delta \tilde{u}_\alpha(\boldsymbol{x}) \Big\} d\Gamma(\boldsymbol{\xi}) d\Gamma(\boldsymbol{x}) \tag{2.17}$$

Substituting Eq.(2.17) into RHS of Eq.(2.1) and Eq.(2.4) into LHS of Eq.(2.1)

$$\frac{4h}{3} \int_\Gamma t_\alpha(\boldsymbol{x}) \Delta \tilde{u}_\alpha(\boldsymbol{x}) d\Gamma(\boldsymbol{x})$$

$$= \int_\Gamma \int_\Gamma \Big\{ \psi_1 \Delta u_\beta(\boldsymbol{\xi}) \Delta \tilde{u}_\alpha(\boldsymbol{x}) + \psi_2 D_3 \Delta u_\beta(\boldsymbol{\xi}) D_3 \Delta \tilde{u}_\alpha(\boldsymbol{x}) \Big\} d\Gamma(\boldsymbol{\xi}) d\Gamma(\boldsymbol{x}) \tag{2.18}$$

We compare Eq.(2.18) with 2D weak-form traction integral equation [2]

$$-\int_\Gamma t_\alpha(\boldsymbol{x}) \Delta \tilde{u}_\alpha(\boldsymbol{x}) d\Gamma(\boldsymbol{x}) = \int_\Gamma \int_\Gamma C^\alpha_\beta D_3 \Delta u_\beta(\boldsymbol{\xi}) D_3 \Delta \tilde{u}_\alpha(\boldsymbol{x}) d\Gamma(\boldsymbol{\xi}) d\Gamma(\boldsymbol{x}) \tag{2.19}$$

to see that Eq.(2.18) is an extended version of Eq.(2.19) in the sense that

$$-\int_\Gamma t_\alpha(\boldsymbol{x}) \Delta \tilde{u}_\alpha(\boldsymbol{x}) d\Gamma(\boldsymbol{x})$$

$$= \int_\Gamma \int_\Gamma \Big\{ C^\alpha_\beta \Delta u_\beta(\boldsymbol{\xi}) \Delta \tilde{u}_\alpha(\boldsymbol{x}) + E^\alpha_\beta D_3 \Delta u_\beta(\boldsymbol{\xi}) D_3 \Delta \tilde{u}_\alpha(\boldsymbol{x}) \Big\} d\Gamma(\boldsymbol{\xi}) d\Gamma(\boldsymbol{x}) \tag{2.20}$$

with the added term E^α_β such that

$$C^\alpha_\beta = -\frac{3}{4h}\psi_1 = -\frac{3Ak}{h^5}\phi_1 - \frac{3Ak}{h^5}\phi_2 - \frac{3Bk}{h^5}\phi_3$$

$$E^\alpha_\beta = -\frac{3}{4h}\psi_2 = -\frac{3Ck}{4h^3}\rho_\beta \rho_\alpha - \frac{3Dk}{4h^3}\delta_{\alpha\beta}$$

2.1.2 $F(x_3,h)=1-\frac{x_3^4}{h^4}$ and $F(\xi_3,h)=1-\frac{\xi_3^4}{h^4}$

We introduce the following constraint on crack profile in x_3 and ξ_3 directions and follow the same process as in quadratic profile

$$\Delta\tilde{u}_\alpha^o(x_1,x_2,x_3)=(1-\frac{x_3^4}{h^4})\Delta\tilde{u}_\alpha(x_1,x_2)$$

$$\Delta u_\beta^o(\xi_1,\xi_2,\xi_3)=(1-\frac{\xi_3^4}{h^4})\Delta u_\beta(\xi_1,\xi_2)$$

The weak form traction integral equation becomes

$$-\int_\Gamma t_\alpha(\boldsymbol{x})\Delta\tilde{u}_\alpha(\boldsymbol{x})d\Gamma(\boldsymbol{x})$$

$$=\int_\Gamma\int_\Gamma\left\{C_\beta^\alpha\Delta u_\beta(\boldsymbol{\xi})\Delta\tilde{u}_\alpha(\boldsymbol{x})+E_\beta^\alpha D_3\Delta u_\beta(\boldsymbol{\xi})D_3\Delta\tilde{u}_\alpha(\boldsymbol{x})\right\}d\Gamma(\boldsymbol{\xi})d\Gamma(\boldsymbol{x})$$

$$C_\beta^\alpha=-\frac{5}{8h}\psi_1$$

$$E_\beta^\alpha=-\frac{5}{8h}\psi_2$$

ϕ_1,ϕ_2,ϕ_3 are same as in quadratic profile and ψ_1,ψ_2,A,B,C,D are obtained as

$$\psi_1=\frac{16Ak}{h^8}\phi_1+\frac{16Ak}{h^8}\phi_2+\frac{16Bk}{h^8}\phi_3$$

$$\psi_2=\frac{Ck}{h^4}\rho_\beta\rho_\alpha+\frac{Dk}{h^4}\delta_{\alpha\beta}$$

$$A=\frac{1}{3675}\Bigg(24a^{\frac{7}{2}}-2450a^{\frac{3}{2}}h^4+7350a^{\frac{1}{2}}h^6$$
$$+\sqrt{a+4h^2}(-24a^3+48a^2h^2+2306ah^4-2950h^6)$$
$$+105h^5(21a-10h^2)ln\left(\frac{-2h+\sqrt{a+4h^2}}{2h+\sqrt{a+4h^2}}\right)\Bigg)$$

$$B = \frac{1}{175a}\Bigg(-8a^{\frac{7}{2}} + 350a^{\frac{3}{2}}h^4 - 350a^{\frac{1}{2}}h^6 + \sqrt{a+4h^2}(8a^3 - 16a^2h^2 - 302ah^4 + 50h^6) - 210ah^5 ln\left(\frac{-2h+\sqrt{a+4h^2}}{2h+\sqrt{a+4h^2}}\right)\Bigg)$$

$$C = \frac{4}{11025ah^4}\Bigg(4(-8a^{\frac{9}{2}} + 2450a^{\frac{5}{2}}h^4 - 7350a^{\frac{3}{2}}h^6 + \sqrt{a+4h^2}(8a^4 - 16a^3h^2 - 1422a^2h^4 + 3515ah^6 + 980h^8)) - 315ah^5(21a - 10h^2)ln\left(\frac{-2h+\sqrt{a+4h^2}}{2h+\sqrt{a+4h^2}}\right)\Bigg)$$

$$D = -\frac{1}{99225h^4}\Bigg(4(-32a^{\frac{9}{2}} + 10584a^{\frac{5}{2}}h^4 - 88200a^{\frac{3}{2}}h^6 + \sqrt{a+4h^2}(32a^4 - 64a^3h^2 - 10392a^2h^4 + 49193ah^6 + 34496h^8)) + 315ah^5(-189a^2 + 360ah^2 + 448h^4)ln\left(\frac{-2h+\sqrt{a+4h^2}}{2h+\sqrt{a+4h^2}}\right)\Bigg)$$

2.1.3 $F(x_3, h) = 1 - \frac{x_6^2}{h^6}$ and $F(\xi_3, h) = 1 - \frac{\xi_3^6}{h^6}$

We introduce the following constraint on crack profile in x_3 and ξ_3 directions and follow the same process as in quadratic profile

$$\Delta\tilde{u}_\alpha^o(x_1, x_2, x_3) = (1 - \frac{x_3^6}{h^6})\Delta\tilde{u}_\alpha(x_1, x_2)$$

$$\Delta u_\beta^o(\xi_1, \xi_2, \xi_3) = (1 - \frac{\xi_3^6}{h^6})\Delta u_\beta(\xi_1, \xi_2)$$

The weak form traction integral equation becomes

$$-\int_\Gamma t_\alpha(\boldsymbol{x})\Delta\tilde{u}_\alpha(\boldsymbol{x})d\Gamma(\boldsymbol{x})$$

$$= \int_\Gamma \int_\Gamma \left\{ C^\alpha_\beta \Delta u_\beta(\boldsymbol{\xi}) \Delta \tilde{u}_\alpha(\boldsymbol{x}) + E^\alpha_\beta D_3 \Delta u_\beta(\boldsymbol{\xi}) D_3 \Delta \tilde{u}_\alpha(\boldsymbol{x}) \right\} d\Gamma(\boldsymbol{\xi}) d\Gamma(\boldsymbol{x})$$

$$C^\alpha_\beta = -\frac{7}{12h}\psi_1 = -\frac{7Ak}{3h^5}\phi_1 - \frac{7Ak}{3h^5}\phi_2 - \frac{7Bk}{3h^5}\phi_3$$

$$E^\alpha_\beta = -\frac{7}{12h}\psi_2 = -\frac{7Ck}{12h^3}\rho_\beta\rho_\alpha - \frac{7Dk}{12h^3}\delta_{\alpha\beta}$$

ϕ_1,ϕ_2,ϕ_3 are same as in quadratic profile and ψ_1,ψ_2,A,B,C,D are obtained as

$$\psi_1 = \frac{36Ak}{h^{12}}\phi_1 + \frac{36Ak}{h^{12}}\phi_2 + \frac{36Bk}{h^{12}}\phi_3$$

$$\psi_2 = \frac{Ck}{h^6}\rho_\beta\rho_\alpha + \frac{Dk}{h^6}\delta_{\alpha\beta}$$

$$\begin{aligned} A = \frac{1}{2401245}\Bigg(& 640a^{\frac{11}{2}} + 853776a^{\frac{5}{2}}h^6 - 8004150a^{\frac{3}{2}}h^8 + 4802490\sqrt{a}h^{10} \\ & + \sqrt{a+4h^2}(-640a^5 + 1280a^4h^2 - 3840a^3h^4 \\ & - 840976a^2h^6 + 4521377ah^8 - 1378566h^{10}) \\ & - \frac{h^7}{2772}(1485a^2 - 3080ah^2 + 504h^4) ln\left(\frac{-2h+\sqrt{a+4h^2}}{2h+\sqrt{a+4h^2}}\right)\Bigg) \end{aligned}$$

$$\begin{aligned} B = \frac{1}{43659a}\Bigg(& 2(-64a^{\frac{11}{2}} - 38808a^{\frac{5}{2}}h^6 + 218295a^{\frac{3}{2}}h^8 - 43659\sqrt{a}h^{10} \\ & + \sqrt{a+4h^2}(64a^5 - 128a^4h^2 + 384a^3h^4 \\ & + 37528a^2h^6 - 104321ah^8 + 3969h^{10})) \\ & + 3465ah^7(27a - 28h^2) ln\left(\frac{-2h+\sqrt{a+4h^2}}{2h+\sqrt{a+4h^2}}\right)\Bigg) \end{aligned}$$

$$C = \frac{1}{6936930ah^6}\Bigg(4(-1280a^{\frac{13}{2}} - 3171168a^{\frac{7}{2}}h^6 + 41621580a^{\frac{5}{2}}h^8 - 41621580a^{\frac{3}{2}}h^{10}$$
$$+ \sqrt{a+4h^2}(1280a^6 - 2560a^5h^2 + 7680a^4h^4 + 3145568a^3h^6$$
$$- 25577041a^2h^8 + 14740488ah^{10} + 2744280h^{12}))$$
$$+ 45045ah^7(495a^2 - 1540ah^2 + 504h^4)ln\left(\frac{-2h + \sqrt{a+4h^2}}{2h + \sqrt{a+4h^2}}\right)\Bigg)$$

$$D = \frac{1}{180360180h^6}\Bigg(-4(-2560a^{\frac{13}{2}} - 11778624a^{\frac{7}{2}}h^6 + 216432216a^{\frac{5}{2}}h^8$$
$$- 360720360a^{\frac{3}{2}}h^{10} + \sqrt{a+4h^2}(2560a^6 - 5120a^5h^2 + 15360a^4h^4$$
$$+ 11727424a^3h^6 - 143188739a^2h^8 + 155053566ah^{10} + 68798664h^{12}))$$
$$- 45045h^7(2145a^3 - 10010a^2h^2 + 6552ah^4 + 6336h^6)ln\left(\frac{-2h + \sqrt{a+4h^2}}{2h + \sqrt{a+4h^2}}\right)\Bigg)$$

2.1.4 $F(x_3, h) = 1 - \frac{x_3^8}{h^8}$ and $F(\xi_3, h) = 1 - \frac{\xi_3^8}{h^8}$

We introduce the following constraint on crack profile in x_3 and ξ_3 directions and follow the same process as in quadratic profile

$$\Delta\tilde{u}_\alpha^o(x_1, x_2, x_3) = (1 - \frac{x_3^8}{h^8})\Delta\tilde{u}_\alpha(x_1, x_2)$$

$$\Delta u_\beta^o(\xi_1, \xi_2, \xi_3) = (1 - \frac{\xi_3^8}{h^8})\Delta u_\beta(\xi_1, \xi_2)$$

The weak form traction integral equation becomes

$$-\int_\Gamma t_\alpha(\boldsymbol{x})\Delta\tilde{u}_\alpha(\boldsymbol{x})d\Gamma(\boldsymbol{x})$$
$$= \int_\Gamma\int_\Gamma \Big\{C_\beta^\alpha\Delta u_\beta(\boldsymbol{\xi})\Delta\tilde{u}_\alpha(\boldsymbol{x}) + E_\beta^\alpha D_3\Delta u_\beta(\boldsymbol{\xi})D_3\Delta\tilde{u}_\alpha(\boldsymbol{x})\Big\}d\Gamma(\boldsymbol{\xi})d\Gamma(\boldsymbol{x})$$

$$C_\beta^\alpha = -\frac{9}{16h}\psi_1 = -\frac{9Ak}{4h^5}\phi_1 - \frac{9Ak}{4h^5}\phi_2 - \frac{9Bk}{4h^5}\phi_3$$

$$E_\beta^\alpha = -\frac{9}{16h}\psi_2 = -\frac{9Ck}{16h^3}\rho_\beta\rho_\alpha - \frac{9Dk}{16h^3}\delta_{\alpha\beta}$$

ϕ_1,ϕ_2,ϕ_3 are same as in quadratic profile and ψ_1,ψ_2,A,B,C,D are obtained as

$$\psi_1 = \frac{64Ak}{h^{16}}\phi_1 + \frac{64Ak}{h^{16}}\phi_2 + \frac{64Bk}{h^{16}}\phi_3$$

$$\psi_2 = \frac{Ck}{h^8}\rho_\beta\rho_\alpha + \frac{Dk}{h^8}\delta_{\alpha\beta}$$

$$\begin{aligned} A = \frac{1}{579729150}\Bigg(& 7168a^{\frac{15}{2}} - 132509520a^{\frac{7}{2}}h^8 + 2597186592a^{\frac{5}{2}}h^{10} \\ & - 4509004500a^{\frac{3}{2}}h^{12} + 1159458300\sqrt{a}h^{14} \\ & + \sqrt{a+4h^2}(-7168a^7 + 14336a^6h^2 - 43008a^5h^4 \\ & + 143360a^4h^6 + 132007760a^3h^8 - 1733148171a^2h^{10} \\ & + 1952030322ah^{12} - 264282876h^{14}) \\ & + \frac{h^9}{51480}(25025a^3 - 122850a^2h^2 + 83160ah^4 - 6864h^6)ln\left(\frac{-2h+\sqrt{a+4h^2}}{2h+\sqrt{a+4h^2}}\right)\Bigg) \end{aligned}$$

$$\begin{aligned} B = \frac{1}{11042460a}\Bigg(& 4(-512a^{\frac{15}{2}} + 4416984a^{\frac{7}{2}}h^8 - 61837776a^{\frac{5}{2}}h^{10} \\ & + 64414350a^{\frac{3}{2}}h^{12} - 5521230\sqrt{a}h^{14} + \sqrt{a+4h^2}(512a^7 - 1024a^6h^2 \\ & + 3072a^5h^4 - 10240a^4h^6 - 4381184a^3h^8 + 38335545a^2h^{10} \\ & - 22827618ah^{12} + 368082h^{14})) \\ & - 45045ah^9(715a^2 - 2340ah^2 + 792h^4)ln\left(\frac{-2h+\sqrt{a+4h^2}}{2h+\sqrt{a+4h^2}}\right)\Bigg) \end{aligned}$$

$$C = \frac{1}{4927697775ah^8}\Bigg(4(-57344a^{\frac{17}{2}} + 2002366080a^{\frac{9}{2}}h^8 - 50459625216a^{\frac{7}{2}}h^{10} + 122644922400a^{\frac{5}{2}}h^{12} - 52562109600a^{\frac{3}{2}}h^{14} + \sqrt{a+4h^2}(57344a^8 - 114688a^7h^2 + 344064a^6h^4 - 1146880a^5h^6 - 1998352000a^4h^8 + 35286637563^3ah^{10} - 58991025456a^2h^{12} + 15085472688ah^{14} + 2061259200h^{16})) - 765765ah^9(25025a^3 - 163800a^2h^2 + 166320ah^4 - 27456h^6)ln\left(\frac{-2h+\sqrt{a+4h^2}}{2h+\sqrt{a+4h^2}}\right)\Bigg)$$

$$D = -\frac{1}{670166897400h^8}\Bigg(4(-458752a^{\frac{17}{2}} + 30257976320a^{\frac{9}{2}}h^8 - 980358432768a^{\frac{7}{2}}h^{10} + 3335941889280a^{\frac{5}{2}}h^{12} - 2382815635200a^{\frac{3}{2}}h^{14} + \sqrt{a+4h^2}(458752a^8 - 917504a^7h^2 + 2752512a^6h^4 - 9175040a^5h^6 - 30225863680a^4h^8 + 714983204779^3ah^{10} - 1765915566888a^2h^{12} + 848488230304ah^{14} + 269233169920h^{16})) + 765765h^9(-425425a^4 + 3712800a^3h^2 - 5654880a^2h^4 + 1867008ah^6 + 1464320h^8)ln\left(\frac{-2h+\sqrt{a+4h^2}}{2h+\sqrt{a+4h^2}}\right)\Bigg)$$

2.2 Comparison to the 2D equation

We need to take a limit as h tends to infinity to see how the RHS of Eq.2.20 reduces to the 2-D case [2].

2.2.1 $F(x_3, h) = 1 - \frac{x_3^2}{h^2}$ and $F(\xi_3, h) = 1 - \frac{\xi_3^2}{h^2}$

We use the following

$$\lim_{h\to\infty} C_\beta^\alpha = \lim_{h\to\infty} -\frac{3}{4h}\psi_1 = 0$$

$$\lim_{h\to\infty} E_\beta^\alpha = \lim_{h\to\infty} -\frac{3}{4h}\psi_2 = \lim_{h\to\infty} -\frac{3Ck}{4h^3}\rho^2\frac{\partial\rho}{\partial\xi_\alpha}\frac{\partial\rho}{\partial\xi_\beta} - \lim_{h\to\infty}\frac{3Dk}{4h^3}\delta_{\alpha\beta}$$
$$= \frac{E}{4\pi(1-\nu^2)}\left[\frac{4}{5}\delta_{\alpha\beta}ln\rho - \frac{4}{5}\frac{\partial\rho}{\partial\xi_\alpha}\frac{\partial\rho}{\partial\xi_\beta}\right]$$

Thus we obtain limit as h tends to infinity of RHS of Eq.2.20 as

$$\lim_{h\to\infty}\int_\Gamma\int_\Gamma\left\{C_\beta^\alpha\Delta u_\beta(\boldsymbol{\xi})\Delta\tilde{u}_\alpha(\boldsymbol{x}) + E_\beta^\alpha D_3\Delta u_\beta(\boldsymbol{\xi})D_3\Delta\tilde{u}_\alpha(\boldsymbol{x})\right\}d\Gamma(\boldsymbol{\xi})d\Gamma(\boldsymbol{x})$$

$$= \int_\Gamma\int_\Gamma\left\{\lim_{h\to\infty} C_\beta^\alpha\Delta u_\beta(\boldsymbol{\xi})\Delta\tilde{u}_\alpha(\boldsymbol{x}) + \lim_{h\to\infty} E_\beta^\alpha D_3\Delta u_\beta(\boldsymbol{\xi})D_3\Delta\tilde{u}_\alpha(\boldsymbol{x})\right\}d\Gamma(\boldsymbol{\xi})d\Gamma(\boldsymbol{x})$$

$$= \int_\Gamma D_3\Delta\tilde{u}_\alpha(\boldsymbol{x})\int_\Gamma 0.8\times\frac{E}{4\pi(1-\nu^2)}\left[\delta_{\alpha\beta}ln\rho - \frac{\partial\rho}{\partial\xi_\alpha}\frac{\partial\rho}{\partial\xi_\beta}\right]D_3\Delta\tilde{u}_\beta(\boldsymbol{\xi})d\Gamma(\boldsymbol{\xi})d\Gamma(\boldsymbol{x}) \tag{2.21}$$

We rewrite Eq.2.20 as

$$-\int_\Gamma t_\alpha(\boldsymbol{x})\Delta\tilde{u}_\alpha(\boldsymbol{x})d\Gamma(\boldsymbol{x})$$

$$= \int_\Gamma D_3\Delta\tilde{u}_\alpha(\boldsymbol{x})\int_\Gamma 0.8\times\frac{E}{4\pi(1-\nu^2)}\left[\delta_{\alpha\beta}ln\rho - \frac{\partial\rho}{\partial\xi_\alpha}\frac{\partial\rho}{\partial\xi_\beta}\right]D_3\Delta\tilde{u}_\beta(\boldsymbol{\xi})d\Gamma(\boldsymbol{\xi})d\Gamma(\boldsymbol{x}) \tag{2.22}$$

We compare this to the 2-D case [2]

$$-\int_{\Gamma} t_\alpha(\boldsymbol{x})\Delta\tilde{u}_\alpha(\boldsymbol{x})d\Gamma(\boldsymbol{x})$$

$$= \int_{\Gamma} D_3\Delta\tilde{u}_\alpha(\boldsymbol{x}) \int_{\Gamma} \frac{E}{4\pi(1-\nu^2)}\left[\delta_{\alpha\beta} ln\rho - \frac{\partial\rho}{\partial\xi_\alpha}\frac{\partial\rho}{\partial\xi_\beta}\right] D_3\Delta\tilde{u}_\beta(\boldsymbol{\xi})d\Gamma(\boldsymbol{\xi})d\Gamma(\boldsymbol{x}) \tag{2.23}$$

to observe that the kernel obtained by modified model for plane strain ($\lim_{h\to\infty}$) is 0.8 times kernel obtained in 2D case [2].

2.2.2 $F(x_3,h) = 1-\frac{x_3^4}{h^4}$ and $F(\xi_3,h) = 1-\frac{\xi_3^4}{h^4}$

$$-\int_{\Gamma} t_\alpha(\boldsymbol{x})\Delta\tilde{u}_\alpha(\boldsymbol{x})d\Gamma(\boldsymbol{x})$$

$$= \int_{\Gamma} D_3\Delta\tilde{u}_\alpha(\boldsymbol{x}) \int_{\Gamma} 0.8888\times\frac{E}{4\pi(1-\nu^2)}\left[\delta_{\alpha\beta} ln\rho - \frac{\partial\rho}{\partial\xi_\alpha}\frac{\partial\rho}{\partial\xi_\beta}\right] D_3\Delta\tilde{u}_\beta(\boldsymbol{\xi})d\Gamma(\boldsymbol{\xi})d\Gamma(\boldsymbol{x})$$

We observe that the kernel obtained by modified model for plane strain ($\lim_{h\to\infty}$) is 0.8888 times kernel obtained in 2D case [2].

2.2.3 $F(x_3,h) = 1-\frac{x_3^6}{h^6}$ and $F(\xi_3,h) = 1-\frac{\xi_3^6}{h^6}$

$$-\int_{\Gamma} t_\alpha(\boldsymbol{x})\Delta\tilde{u}_\alpha(\boldsymbol{x})d\Gamma(\boldsymbol{x})$$

$$= \int_{\Gamma} D_3\Delta\tilde{u}_\alpha(\boldsymbol{x}) \int_{\Gamma} 0.9231\times\frac{E}{4\pi(1-\nu^2)}\left[\delta_{\alpha\beta} ln\rho - \frac{\partial\rho}{\partial\xi_\alpha}\frac{\partial\rho}{\partial\xi_\beta}\right] D_3\Delta\tilde{u}_\beta(\boldsymbol{\xi})d\Gamma(\boldsymbol{\xi})d\Gamma(\boldsymbol{x})$$

We observe that the kernel obtained by modified model for plane strain ($\lim_{h\to\infty}$) is 0.9231 times kernel obtained in 2D case [2].

2.2.4 $F(x_3, h) = 1 - \frac{x_3^8}{h^8}$ and $F(\xi_3, h) = 1 - \frac{\xi_3^8}{h^8}$

$$- \int_\Gamma t_\alpha(\boldsymbol{x}) \Delta\tilde{u}_\alpha(\boldsymbol{x}) d\Gamma(\boldsymbol{x})$$

$$= \int_\Gamma D_3 \Delta\tilde{u}_\alpha(\boldsymbol{x}) \int_\Gamma 0.9412 \times \frac{E}{4\pi(1-\nu^2)} \left[\delta_{\alpha\beta} ln\rho - \frac{\partial\rho}{\partial\xi_\alpha} \frac{\partial\rho}{\partial\xi_\beta} \right] D_3 \Delta\tilde{u}_\beta(\boldsymbol{\xi}) d\Gamma(\boldsymbol{\xi}) d\Gamma(\boldsymbol{x})$$

We observe that the kernel obtained by modified model for plane strain ($\lim_{h\to\infty}$) is 0.9412 times kernel obtained in 2D case [2].

2.3 Crack Tip Elements and Shape Functions

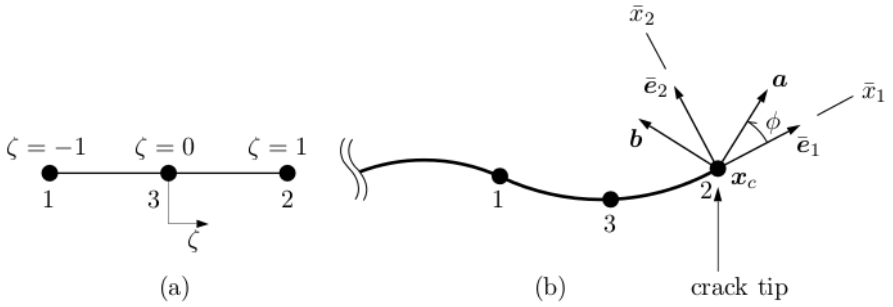

Figure 2.3: Master Element (a) and Crack Tip Element (b)

Since Eq.2.20 has weakly singular ($O(ln\ \rho)$) kernels C_β^α and E_β^α, it is sufficient to utilize standard isoparametric C^0 elements. Since we only work with 3-noded elements, we use quadratic shape functions. Special shape functions $\psi_i'(\zeta)$ are used for crack tip elements to more accurately model the behavior of the crack opening displacements as shown in Figure 2.3.

$$\psi_i'(\zeta) = \frac{\sqrt{1-\zeta}}{A_i(\zeta)} \psi_i(\zeta) \qquad \text{(no sum on } i\text{)}$$

where $\psi_i(\zeta)$ are the standard 3-node quadratic shape functions associated with the i^{th} node, and

$$A_i(\zeta) = \begin{cases} \sqrt{1-\zeta_i} & \text{for} \quad \zeta_i \neq 1 \\ \frac{1}{2} & \text{for} \quad \zeta_i = 1 \end{cases}$$

in which ζ_i is the coordinate on the master element of the i^{th} node. In the above formulation, $\psi = 1$ is associated with the crack tip node. For the case that $\psi = -1$ is the crack tip node, the expressions for ψ_i' and A_i are analogous, but simply have the $1-\zeta$ terms replaced with $1+\zeta$. The opening displacements on the crack tip element can be interpolated as

$$\Delta \boldsymbol{u} = \sqrt{1-\zeta} \sum_{i=1}^{3} \frac{\boldsymbol{u}_i}{A_i} \psi_i(\zeta)$$

where $\boldsymbol{u}_i$ are the unknown displacements of the i^{th} node. Additionally,the stress intensity factors depend on the opening displacements near the crack tip. Thus using special square-root shape functions also allows us to directly compute stress intensity factors from the opening displacements without relying on post-processing.

2.4 Crack Growth Criteria

In HyFrac2D, the crack growth is governed by the maximum hoop stress at the crack tip, which determines the direction and magnitude of the crack advance. Consider our crack tip coordinate system shown in Figure 2.4. Axis 1 is in the tangential direction of the crack surface and directs into the material.

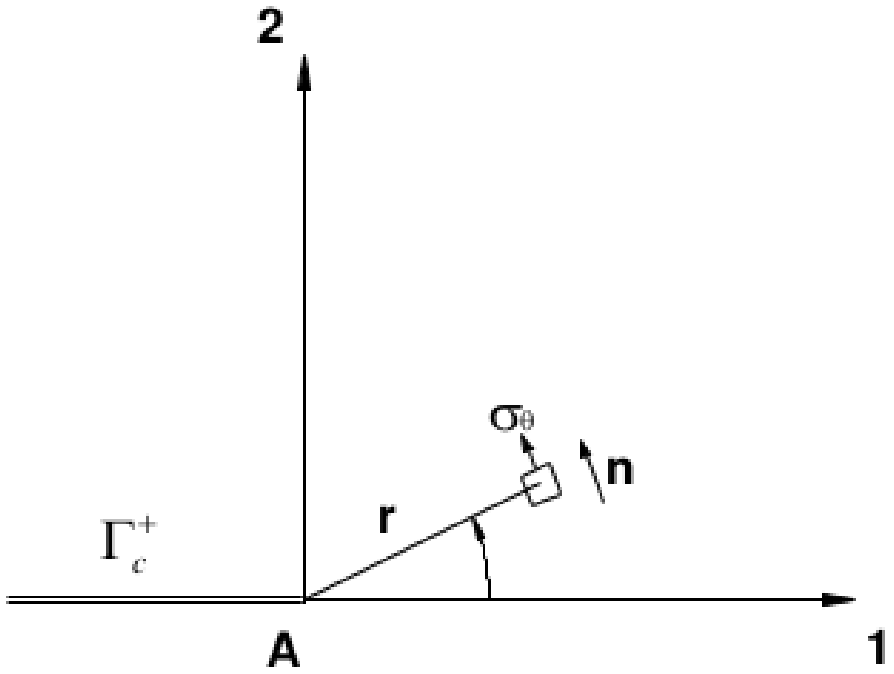

Figure 2.4: Crack Tip Coordinate System

Axis 2 is normal to axis 1 and directs in the opposite direction of the normal vector of the positive crack face, Γ_c^+, which is defined by the order of nodes of crack elements. We also note that σ_θ is the normal, or hoop, stress and $\mathbf{n}$ is the unit normal vector in the θ-direction.

Let Δa denote the crack advance at a given crack tip and let θ_g be the angle of growth. The growth direction is then given by

$$\tan\left(\frac{\theta_g}{2}\right) = \frac{K_I - \sqrt{K_I^2 + 8K_{II}^2}}{4K_{II}}, \qquad -\pi \leq \theta_g \leq \pi$$

where K_I and K_{II} are the mode-I and mode-II stress intensity factors respec-

tively. The growth of each crack tip is then given by the following bi-linear growth law

$$\frac{\Delta a}{\Delta a_0} = \begin{cases} 0 & , \quad \frac{\bar{K}_I}{K_{IC}} < 1-\beta \\ \frac{1-\alpha}{\beta-\alpha}\left(\frac{\bar{K}_I}{K_{IC}} - 1 + \beta\right) & , \quad 1-\beta \leq \frac{\bar{K}_I}{K_{IC}} < 1-\alpha \\ \frac{\bar{K}_I}{K_{IC}} & , \quad 1-\alpha \leq \frac{\bar{K}_I}{K_{IC}} \end{cases}$$

where $\bar{K}_I$ is an equivalent mode-I stress intensity factor defined by

$$\bar{K}_I = K_I \cos^3\left(\frac{\theta_g}{2}\right) - \frac{3}{2} K_{II} \cos\left(\frac{\theta_g}{2}\right) \sin\theta_g \tag{2.24}$$

in which K_{IC} is the fracture toughness, and $\{\Delta a_0, \alpha, \beta\}$ are user-defined model constants. To prevent computational error when $\bar{K}_I$ at a given tip is very close to K_{IC}, we also require an additional user-defined parameter ε such that

$$1 - \varepsilon \leq \frac{\bar{K}_I}{K_{IC}} \leq 1 \Rightarrow \frac{\Delta a}{\Delta a_0} = 1 \tag{2.25}$$

The bi-linear crack growth law can be visualized in Figure 2.5.

For each load step, $\bar{K}_I$ at each crack tip must not exceed K_{IC} and thus we scale our solution such that the maximum $\bar{K}_I$ is equal to K_{IC}. Thus, Δa_0 serves as the propagation step size for the crack tip with the largest hoop stress, accordingly the advance of the other crack tips is proportional to the ratio of it's equivalent mode-I stress intensity factor to the maximum hoop stress, which is to say the fracture toughness.

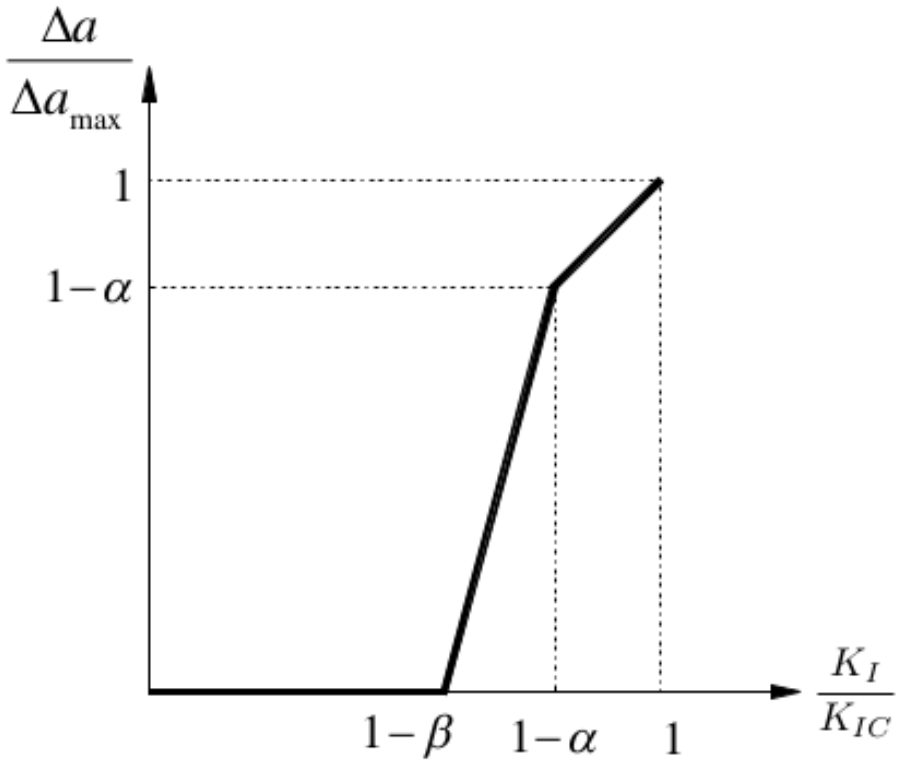

Figure 2.5: Bi-linear Crack Growth Law

2.5 Solution Strategy

We have two solution strategies for investigating the propagation of multiple interacting cracks. We consider n cracks in generally anisotropic elastic media subject to an anisotropic remote stress and internal pressure, constant at each load step, in each crack. Towards modeling the crack propagation, HyFrac2D first uses the solution for a unit pressure to find the crack tip for which the stress intensity factor first reaches the critical SIF, which is to say $\bar{K}_I = K_{IC}$. We then scale the unit pressure to find the pressure at

which this tip first begins to grow. HyFrac2D scales the pressure in each crack and the volumes of each crack accordingly to investigate crack growth as a function of either injection pressure or injection volume.

2.5.1 Linearly Dependent Injection Pressures

We first consider a strategy to simulate crack propagation due to linearly dependent injection pressures. HyFrac2D computes the pressure scaling, α_j^P, necessary to propagate the cracks at each load step. These pressure scaling values are subject to the following stress intensity factor constraint:

$$K_m = K_m^0 + K_{ij}^P \alpha_j^P \qquad (m = 1, \ldots, 2n)$$

Here K_m^0 is the stress intensity factor at crack tip m due to the remote tractions, and K_{ij}^P is the stress intensity factor at crack tip m due to the pressure in crack j.

We also require the pressure scaling values to be linearly dependent and thus can be expressed as $\alpha_j^P = \beta_j^P \alpha_n^P$. In the case of equal injection pressure in each crack, β_j is a vector of ones. We can then calculate the stress intensity factors due to a unit pressure in each crack, scale the stress intensity factors such that the SIF at each tip reaches the critical value, and then take the minimum pressure scaling value to causes the cracks to grow. We find the pressure in the n^{th} crack to be

$$\alpha_n^P = \min\left(\frac{K_{IC} - K_m^0}{K_{mj}^P \beta_j^P}\right).$$

Thus we find the pressure in each crack necessary for crack growth to commence.

2.5.2 Linearly Dependent Injection Volumes

We also consider a strategy to simulate crack propagation due to linearly dependent injection volumes. The pressure scaling values, α_j^P, are now subject to the following stress intensity factor and volume constraints:

$$V_i = V_i^0 + V_{ij}^P \alpha_j^P \qquad (i, j = 1, \ldots, n)$$
$$K_m = K_m^0 + K_{ij}^P \alpha_j^P \qquad (m = 1, \ldots, 2n)$$

Here V_i^0 is the volume of crack i due to the remote tractions, V_{ij}^P is the volume of crack i due to the pressure in crack j, K_m^0 is the stress intensity factor at crack tip m due to the remote tractions, and K_{ij}^P is the stress intensity factor at crack tip m due to the pressure in crack j.

The volume in each crack can then be specified, and taken relative to the volume in the n^{th} crack, such that $V_i = \beta_i^V V_n$. As in the case of prescribed injection pressure, when β_i^V is a vector of ones, then all n cracks have equal volume. Considering the pressure in the n^{th} crack to be specified, we can rewrite our volume constraint as $n - 1$ equations and unknowns

$$\left(V_{ij}^{P} - \beta_i^V V_{nj}^{P}\right) \alpha_j^P = \left(\beta_i^V V_n^0 - V_i^0\right) + \left(\beta_i^V V_{nn}^{P} - V_{in}^{P}\right) \alpha_n^P.$$

This system of equations is of the form

$$A_{ij}\alpha_j^P = L_i + M_i\alpha_n^P,$$

such that $A_{ij} = V_{ij}^{P} - \beta_i^V V_{nj}^{P}$, $L_i = \beta_i^V V_n^0 - V_i^0$, and $M_i = \beta_i^V V_{nn}^{P} - V_{in}^{P}$ are all known. We can then solve the two linear systems of equations

$$A_{ij}\alpha_j^L = L_i \text{ and } A_{ij}\alpha_j^M = M_i$$

Our pressure solution for our original equation is

$$\alpha_j^P = \alpha_j^L + \alpha_j^M\alpha_n^P.$$

Our last remaining unknown is α_n^P, which we can solve for using the SIF constraint. Substituting our pressure solution into the SIF constraint yields

$$K_m = K_m^0 + K_{ij}^P \left(\alpha_j^L + \alpha_j^M\alpha_n^P\right).$$

Solving for each of the m crack tips, we have

$$\alpha_n^P\,(m) = \frac{K_{IC} - K_m^0 - K_{ij}^P\alpha_j^L}{K_{ij}^P\alpha_j^M}$$

We choose the smallest α_n^P, as this will give us the smallest pressure necessary to initial crack growth. From this pressure solution we can calculate the total tractions, opening displacements, and SIF's for the given load step. We can then calculate the growth of crack crack for the given load step from these stress intensity factors.

Chapter 3

Results

3.1 Testing accuracy of our model

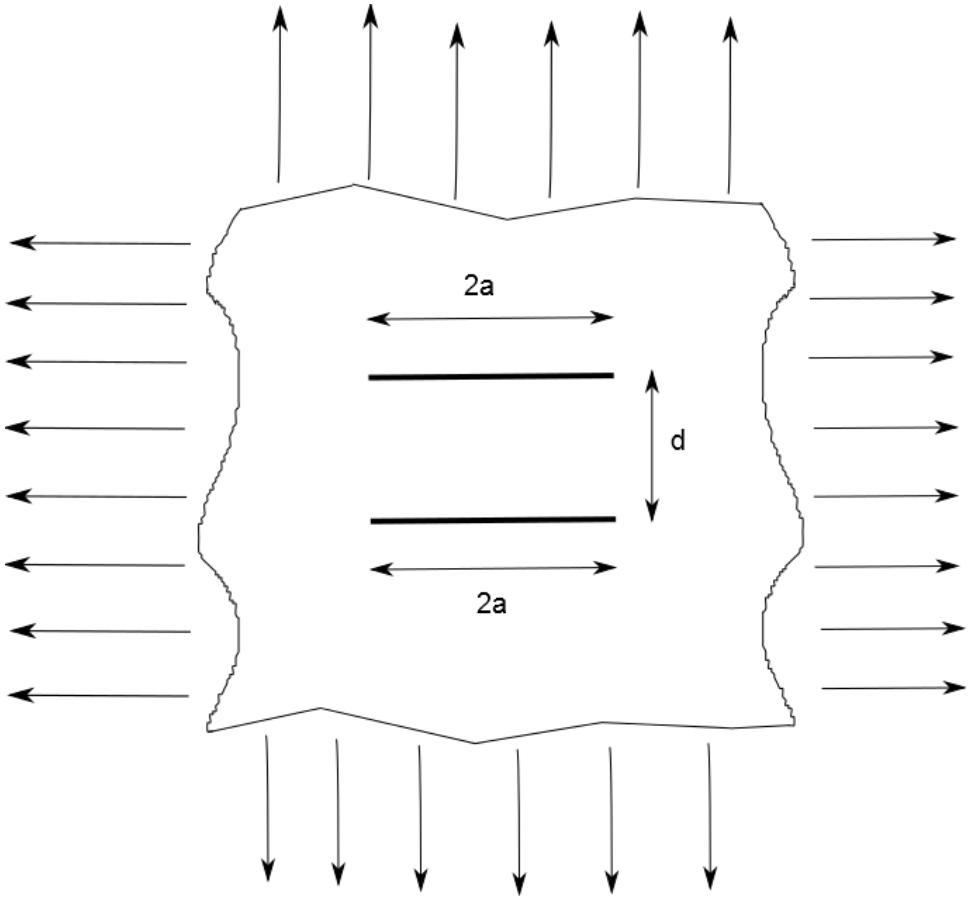

Figure 3.1: Two parallel cracks of length $2a$ separated by distance d subject to uniform remote biaxial tension σ_0.

We test model accuracy for two parallel cracks as shown in Figure 3.1 in near plane strain with quadratic profile. We expect SIF obtained using HyFrac2D for high value of $\frac{h}{a}$ to be $\frac{1}{0.8} = 1.25$ times the well known analytic solution 2D crack in Murakami's SIF Handbook [3] given by

$$K_I = F_I \sigma_0 \sqrt{\pi a}$$

$$F_I = 1 - 0.0007\lambda - 0.4130\lambda^2 + 0.2687\lambda^3 \qquad | \qquad \lambda = \frac{2a}{d}.$$

1. For $\lambda = \frac{2}{3}$ and $a = 2$, Murakami solution is $K_I = 2.2449\sigma_0$. Using HyFrac2D with $\frac{h}{a} = 100$, we get $K_I = 2.8078\sigma_0$, which is a difference of 0.06% from the expected value of $1.25 \times 2.2449\sigma_0 = 2.8601\sigma_0$.

2. For $\lambda = 1$ and $a = 2$, Murakami solution is $K_I = 2.1432\sigma_0$. Using HyFrac2D with $\frac{h}{a} = 100$, we get $K_I = 2.6420\sigma_0$, which is a difference of 1.38% from the expected value of $1.25 \times 2.1432\sigma_0 = 2.6790\sigma_0$.

3.2 Variation in SIF with crack height and crack profile

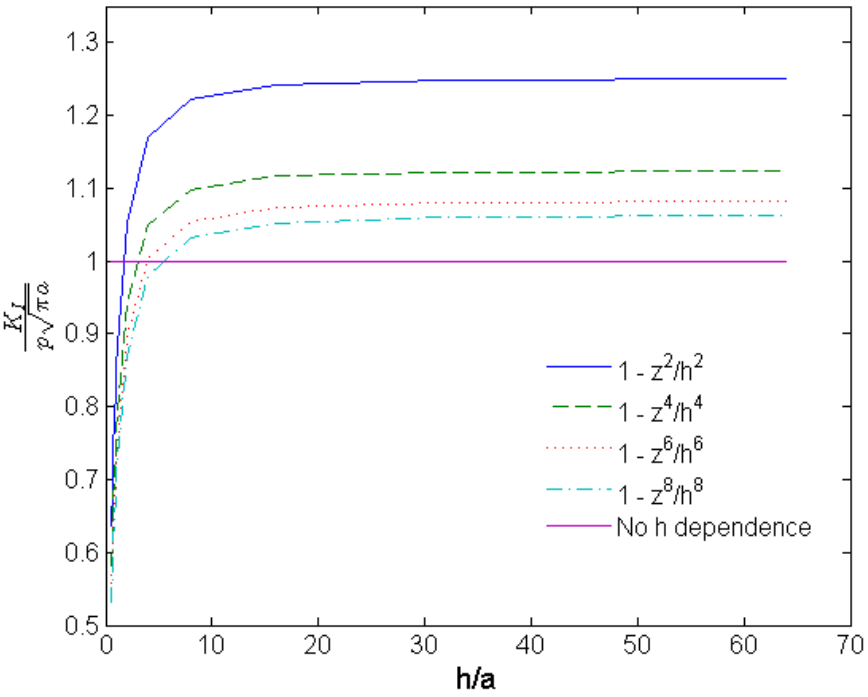

Figure 3.2: $\frac{K_I}{p\sqrt{\pi a}}$ versus $\frac{h}{a}$ for single crack of length $2a$ with $(1-\frac{z^2}{h^2})$, $(1-\frac{x^4}{h^4})$, $(1-\frac{x^6}{h^6})$ and $(1-\frac{x^8}{h^8})$ profiles.

We apply pressure p and zero remote stress to a single crack of length $2a$ and height $2h$ and plot the normalized SIF $(\frac{K_I}{p\sqrt{\pi a}})$ against dimensionless quantity $(\frac{h}{a})$ for all four profiles as shown in Figure 3.2.

1. A monotonic increase in K_I is observed with increasing h which indicates that material is more resistant to crack growth for shorter cracks.

2. K_I plateaus to $\frac{1}{0.8} = 1.25$, $\frac{1}{0.8888} = 1.125$, $\frac{1}{0.9231} = 1.0833$ and $\frac{1}{0.9412} =$

1.0625 times 2D result for $(1-\frac{z^2}{h^2})$,$(1-\frac{z^4}{h^4})$,$(1-\frac{z^6}{h^6})$ and $(1-\frac{z^8}{h^8})$ profiles.

3.3 Variation in crack pressure and volume with crack height

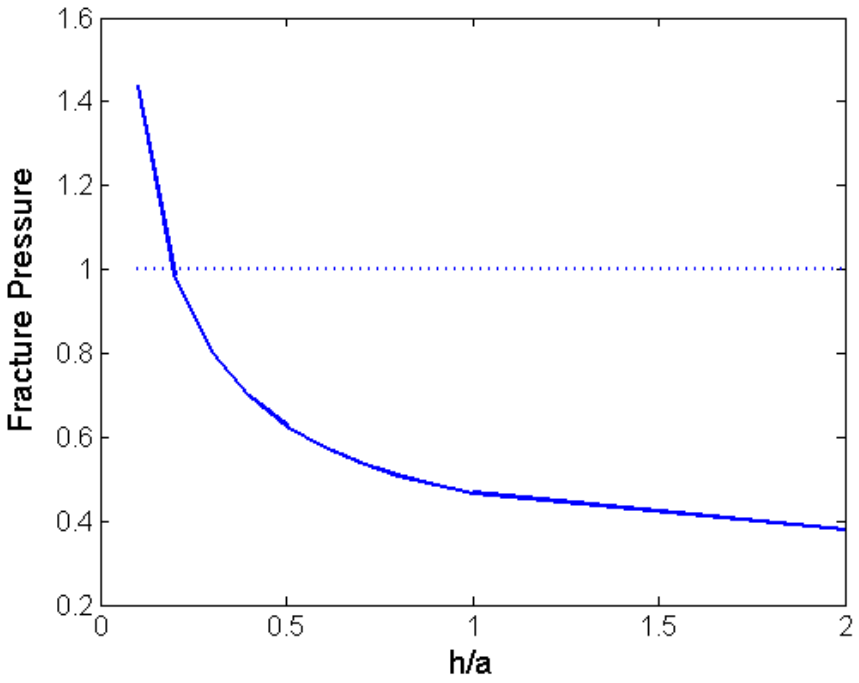

Figure 3.3: Pressure necessary for crack growth reduces monotonically as $\frac{h}{a}$ increases. It overshoots the applied unit pressure at $\frac{h}{a} \sim 0.2$ which means that crack will not grow on application of unit pressure. Single crack of length $2a$ with $1-\frac{z^2}{h^2}$ profile.

Figure 3.3 clearly suggests that the crack with increasing height offers decreasing resistance to crack growth. Figure 3.4 clearly suggests that crack with increasing height is more responsive to mode I type loading provided by unit pressure inside crack.

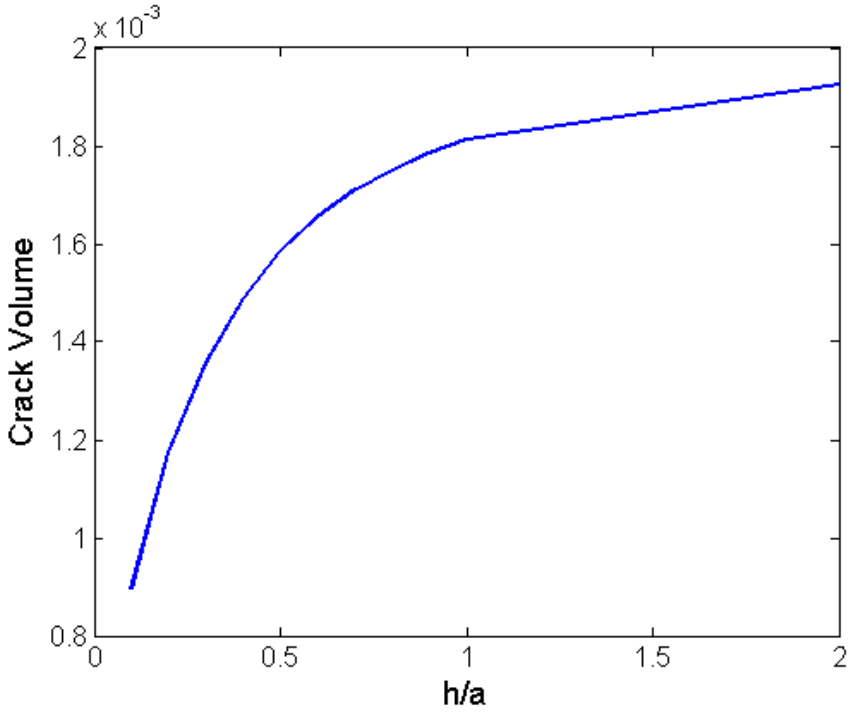

Figure 3.4: Crack volume increases monotonically with increasing $\frac{h}{a}$. Single crack of length $2a$ with $1 - \frac{z^2}{h^2}$ profile.

3.4 Variation in opening displacement with crack height

From Figure 3.5, we observe that gradation in opening displacement across crack length is much smoother for near plane strain crack (high $\frac{h}{a}$) than short crack ($\frac{h}{a} \sim 0.1$). Opening displacement has much flatter trajectory for low $\frac{h}{a}$ characteristic of higher resistance to crack growth.

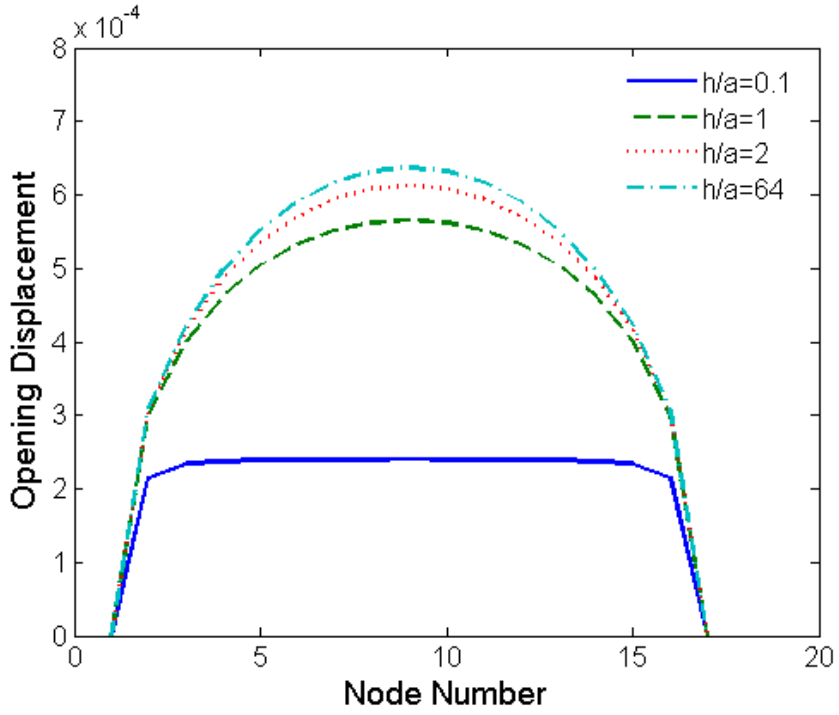

Figure 3.5: Peakedness of opening displacement increases with increasing crack height. Single crack with low $\frac{h}{a}$ exhibits almost similar opening displacement for nodes away from crack tip.

3.5 Crack Growth

Although we just established that near plane strain crack (high $\frac{h}{a}$) offers lesser resistance to crack growth than cracks with comparable height $2h$ to length $2a$ ratio, we need to carefully study crack-crack interaction for results that appear counter-intuitive. It has already been established that two parallel cracks subject to internal pressure grow apart as shown in Figure 3.6 [4]. We plot the advance of crack tip A to A' and study the effect of $\frac{d}{a}$, $\frac{h}{a}$ and crack profile.

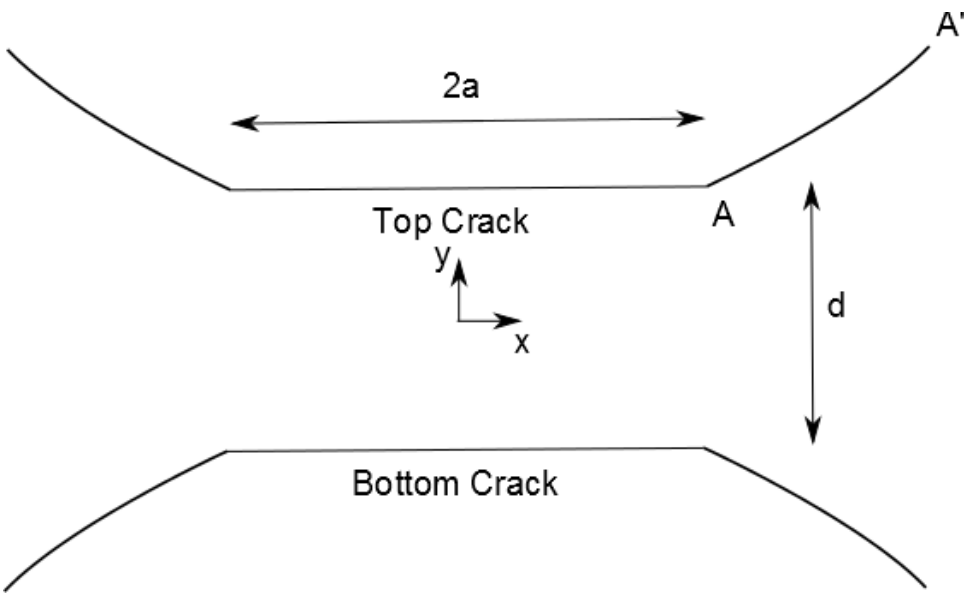

Figure 3.6: Identical crack growth for two aligned cracks.

3.5.1 Two aligned cracks, same $\frac{h}{a}$, different crack profiles

From Figures 3.7 and 3.8, we observe that crack with $1-\frac{z^2}{h^2}$ profile grows more than crack with $1-\frac{z^4}{h^4}$, $1-\frac{z^6}{h^6}$ and $1-\frac{z^8}{h^8}$ profiles for both $\frac{h}{a}=0.5$ and $\frac{h}{a}=1$ although the difference is not appreciable. We always defer to quadratic $1-\frac{z^2}{h^2}$ profile for most purposes.

3.5.2 Two aligned cracks, same $1-\frac{z^2}{h^2}$ profile, different values of $\frac{h}{a}$

Figure 3.9 shows that crack growth is most pronounced for $\frac{h}{a}=1$ when $\frac{d}{a}=0.5$. From Figure 3.10, we observe that crack growth is most significant for $\frac{h}{a}=64$ when $\frac{d}{a}=2$. This suggests that plane strain cracks (high $\frac{h}{a}$) grow the most only when crack-crack interaction is not very important (high $\frac{d}{a}$).

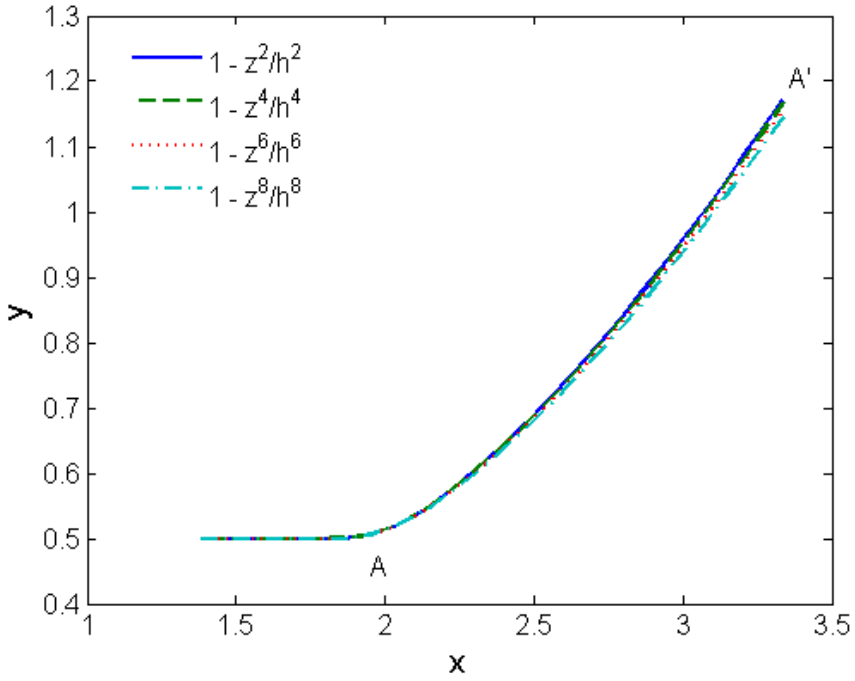

Figure 3.7: Two aligned cracks, $\frac{d}{a} = 0.5$ and $\frac{h}{a} = 0.5$. $a = 2$. Equal injection pressures. Crack with $1 - \frac{z^2}{h^2}$ profile curves up the most.

From Figures 3.11 and 3.12, we observe that drop in fracture pressure for low $\frac{h}{a}$ becomes lot more pronounced at low $\frac{d}{a}$ where crack-crack interaction is important. It has already been established that three parallel cracks subject to internal pressure grow apart as shown in Figure 3.13 [4]. As before, we compare advance of crack tip A for $\frac{h}{a} = 1$ against $\frac{h}{a} = 64$ with $\frac{d}{a} = 0.5$.

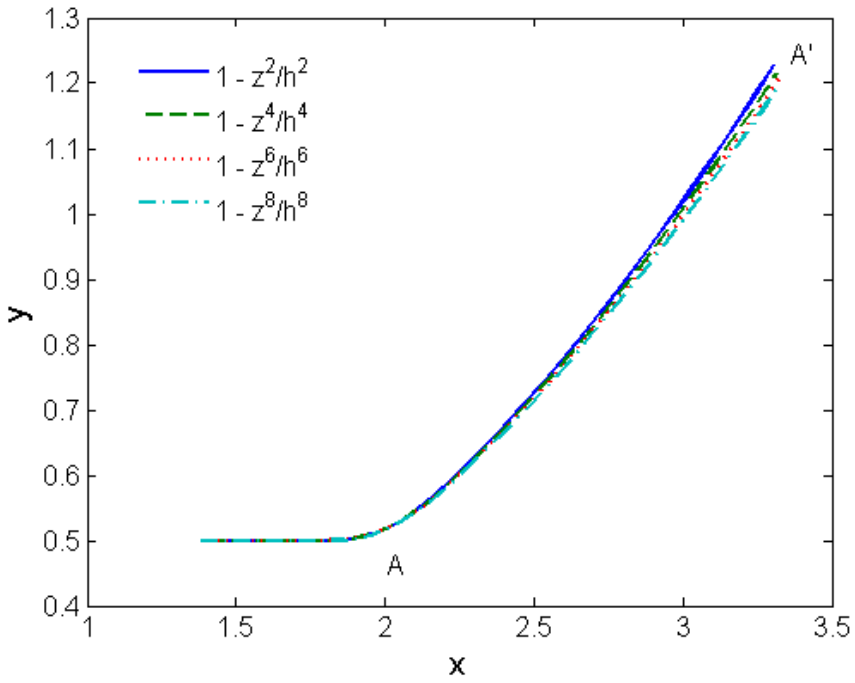

Figure 3.8: Two aligned cracks, $\frac{d}{a} = 0.5$ and $\frac{h}{a} = 1$. $a = 2$. Equal injection pressures. Crack with $1 - \frac{z^2}{h^2}$ profile curves up the most.

3.5.3 Three aligned cracks, same $1-\frac{z^2}{h^2}$ profile, Equal injection pressures, $\frac{h}{a} = 1$ against $\frac{h}{a} = 64$

Figure 3.14 clearly shows that crack with $\frac{h}{a} = 1$ grows faster than near plane strain crack $\frac{h}{a} = 64$. We have now established that crack with comparable height to length ratio ($\frac{h}{a} \sim 1$) grows faster than plane strain crack (high $\frac{h}{a}$) when crack-crack interaction is important ($\frac{d}{a} \sim 0.5$) for both 2 aligned cracks and 3 aligned cracks. We now study the effect of pressure constraint versus volume constraint for the case of 4, 5 and 6 aligned cracks with $\frac{h}{a} = 1$ and $\frac{d}{a} = 0.5$.

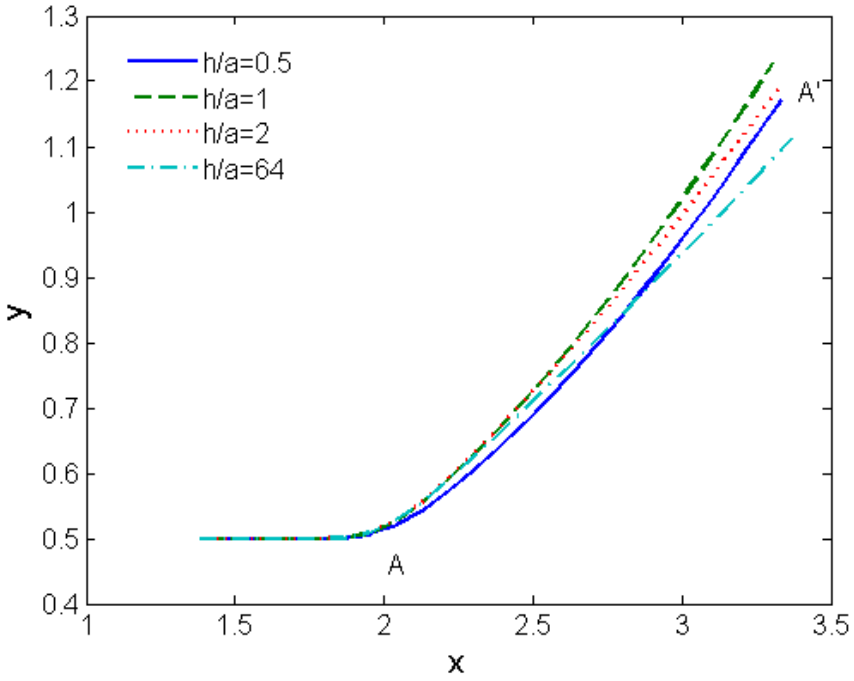

Figure 3.9: Two aligned cracks, $\frac{d}{a} = 0.5$. $a = 2$. Crack with $\frac{h}{a} = 1$ curves up the most.

3.6 Pressure constraint versus Volume constraint

Figures 3.15, 3.17 and 3.19 clearly suggest symmetric growth when subjected to equal injection pressures. Figure 3.16 suggests that the left crack tip grows faster than right crack tip for the case of 4 aligned cracks. Figure 3.18 suggests symmetric behavior for the case of 5 aligned cracks even when subject to equal injection volumes. Figure 3.20 suggests that the inner cracks follow the outer cracks. All these clearly suggest behavior of multiple interacting cracks subject to equal injection volumes is lot more interesting than subject to equal injection pressures.

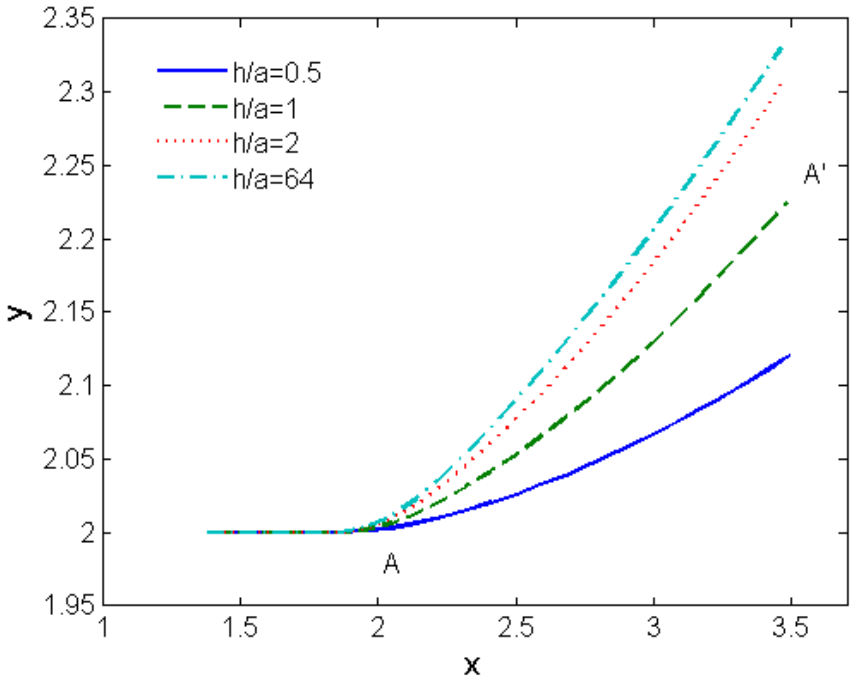

Figure 3.10: Two aligned cracks, $\frac{d}{a} = 2$. $a = 2$. Equal injection pressures. Crack with $\frac{h}{a} = 64$ curves up the most.

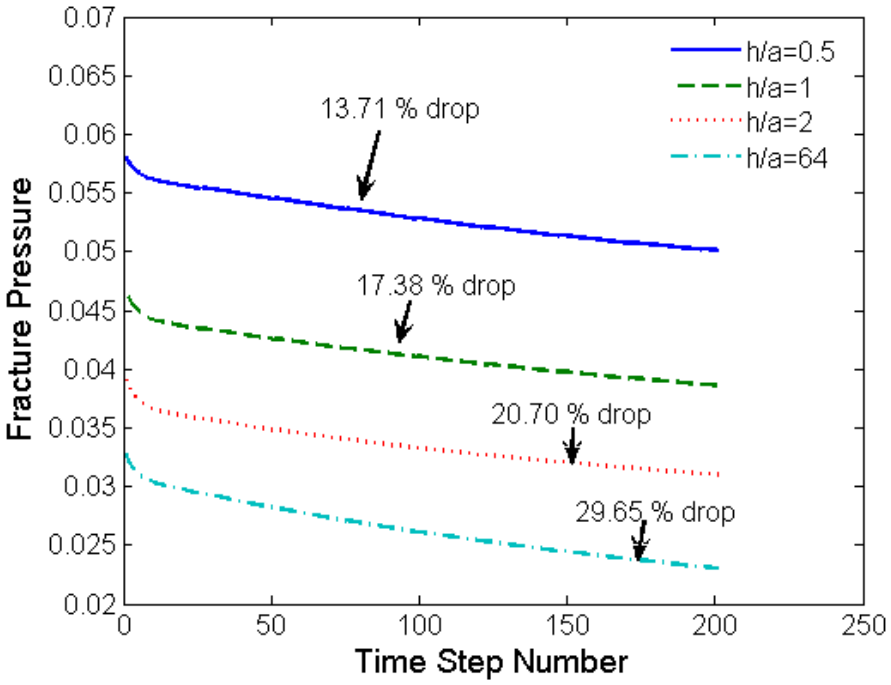

Figure 3.11: Two aligned cracks, $\frac{d}{a} = 0.5$. $a = 2$. Equal injection pressures. Drop in fracture pressure as crack grows. The drop is higher with higher $\frac{h}{a}$.

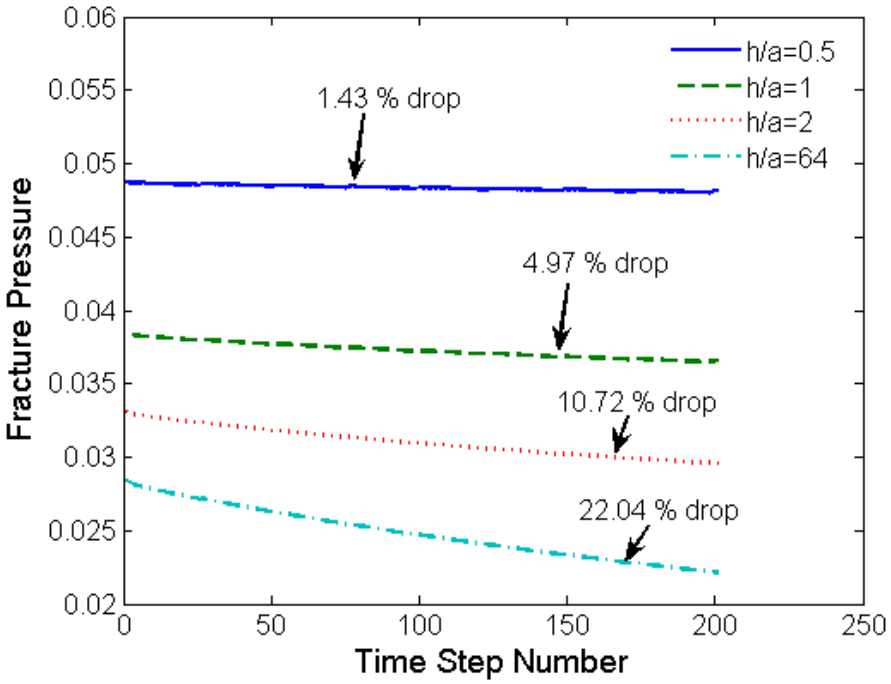

Figure 3.12: Two aligned cracks, $\frac{d}{a} = 2$. $a = 2$. Equal injection pressures. Drop in fracture pressure as crack grows. The drop is higher with higher $\frac{h}{a}$. For $\frac{h}{a} = 0.5$, we observe only 1.43% drop with $\frac{d}{a} = 2$ as opposed to 13.71% drop with $\frac{d}{a} = 0.5$. This suggests that cracks with comparable height to length ratio grow much faster when crack-crack interaction is more active.

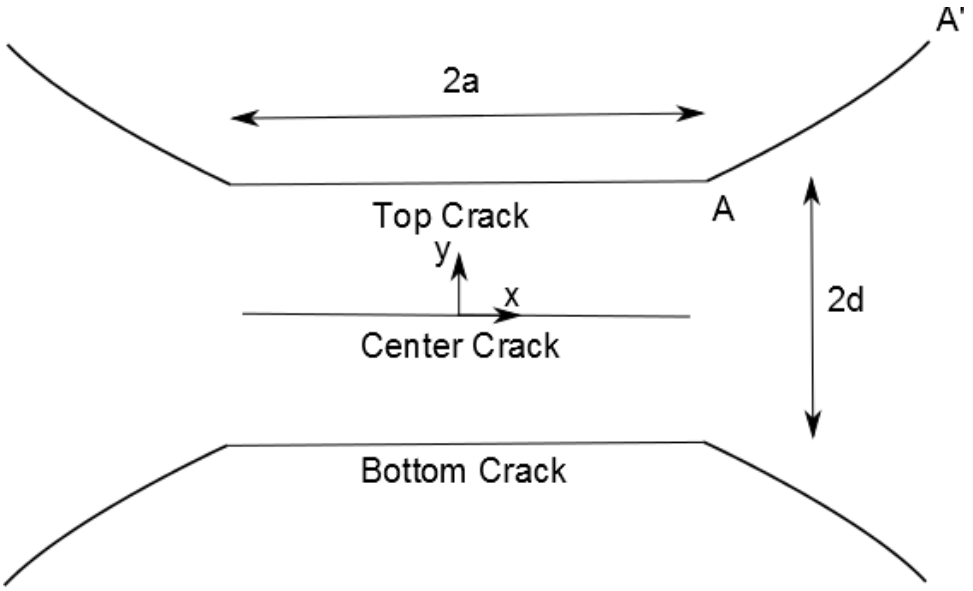

Figure 3.13: Identical crack growth of top and bottom crack for 3 aligned cracks with equal injection pressures.

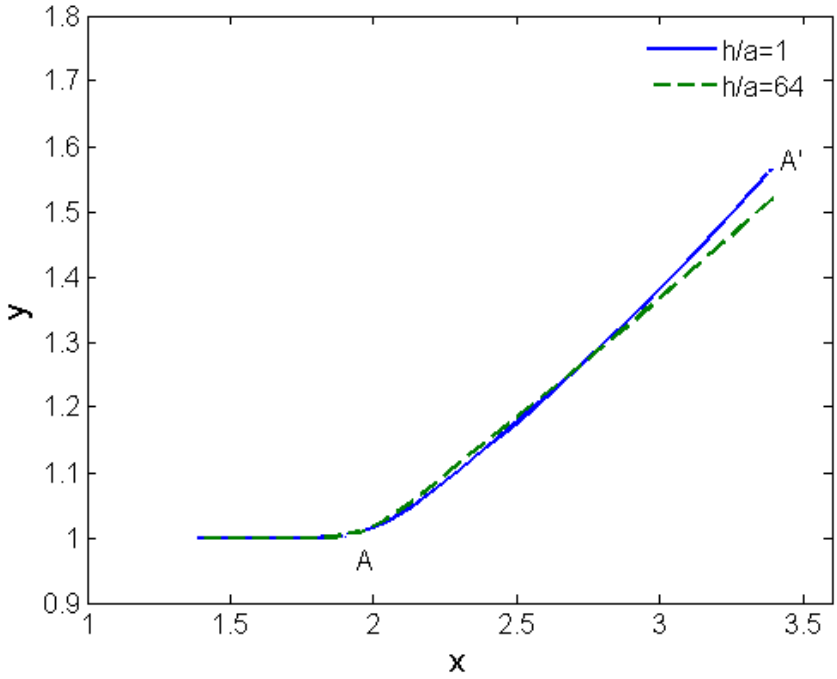

Figure 3.14: Three aligned cracks, $\frac{d}{a} = 0.5$, $a = 2$. Crack with $\frac{h}{a} = 1$ curves up more than crack with $\frac{h}{a} = 64$. This behavior is similar to the case of 2 aligned cracks.

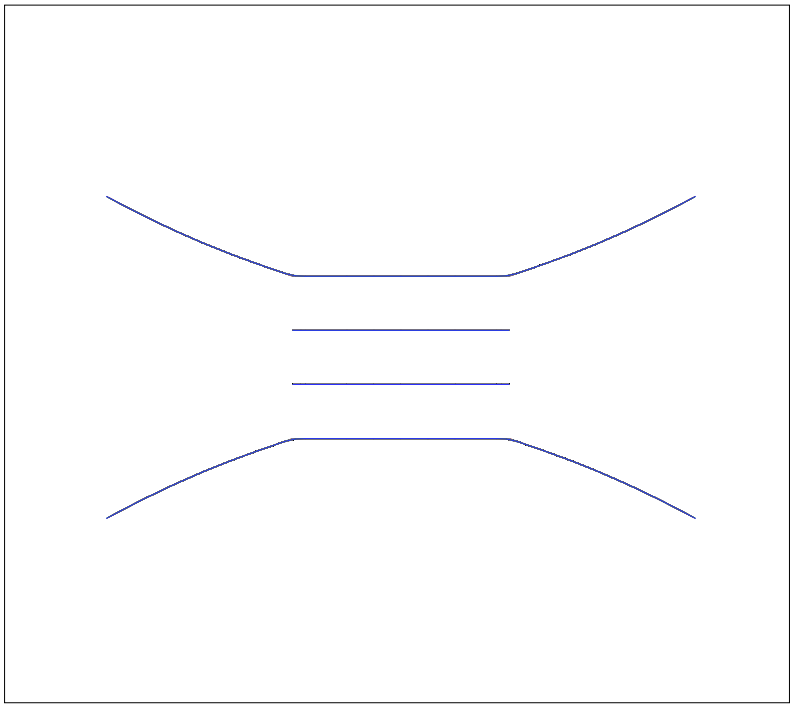

Figure 3.15: Four aligned cracks initially with $\frac{d}{a} = 0.5$, $\frac{h}{a} = 1$ and $a = 2$ grow into this configuration on application of equal injection pressures on the 4 cracks.

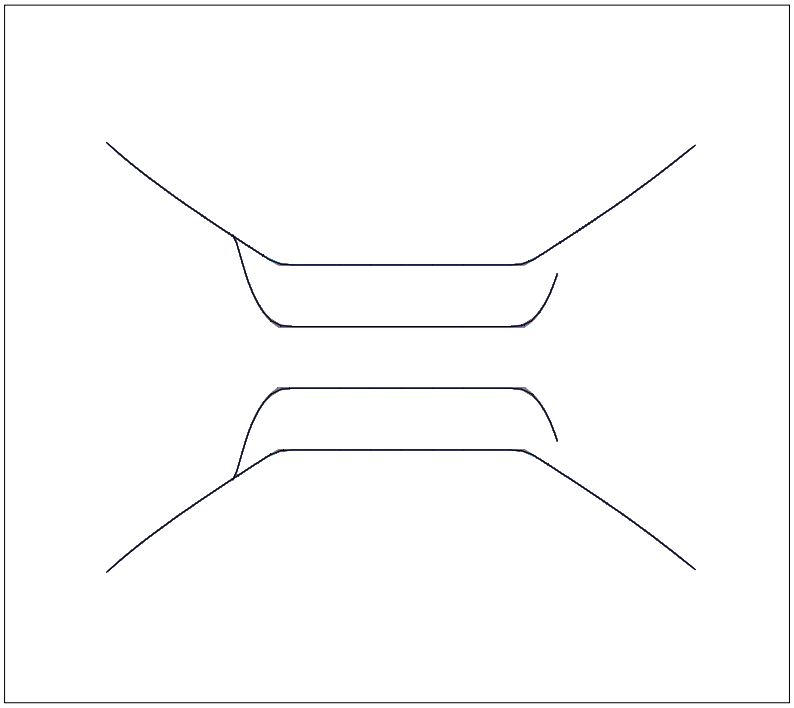

Figure 3.16: Four aligned cracks initially with $\frac{d}{a} = 0.5$, $\frac{h}{a} = 1$ and $a = 2$ grow into this configuration on application of equal injection volumes on the 4 cracks.

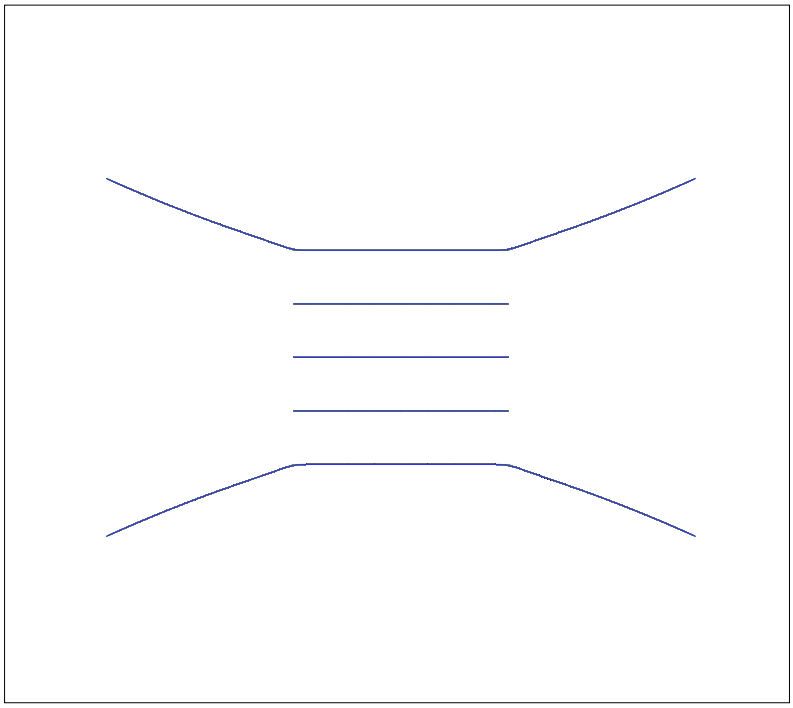

Figure 3.17: Five aligned cracks initially with $\frac{d}{a} = 0.5$, $\frac{h}{a} = 1$ and $a = 2$ grow into this configuration on application of equal injection pressures on the 5 cracks.

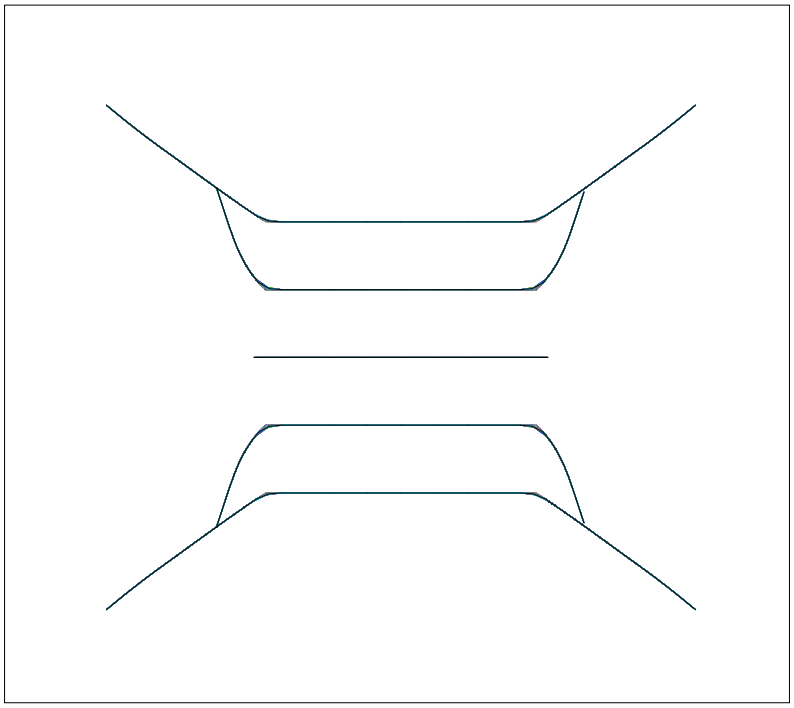

Figure 3.18: Five aligned cracks initially with $\frac{d}{a} = 0.5$, $\frac{h}{a} = 1$ and $a = 2$ grow into this configuration on application of equal injection volumes on the 5 cracks.

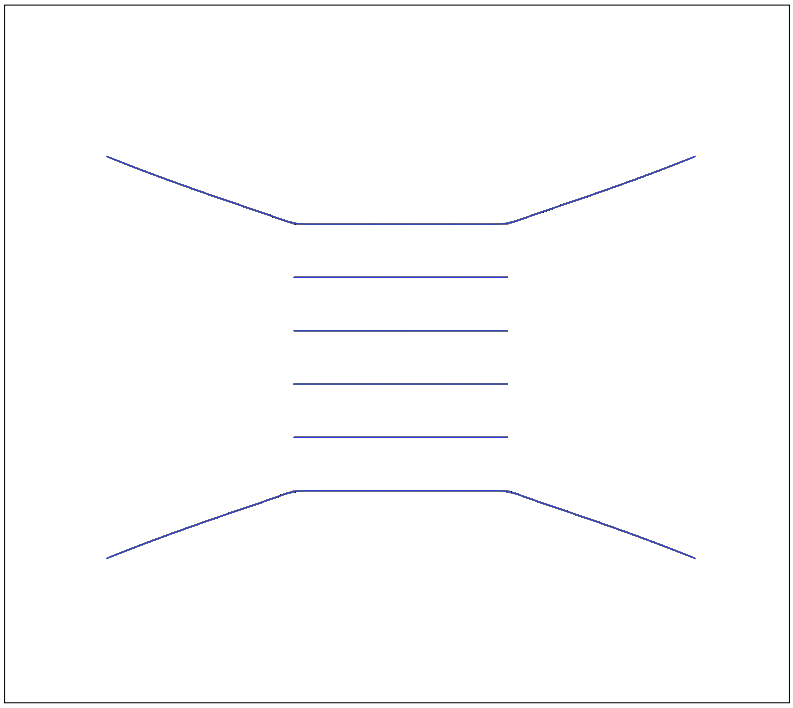

Figure 3.19: Six aligned cracks initially with $\frac{d}{a} = 0.5$, $\frac{h}{a} = 1$ and $a = 2$ grow into this configuration on application of equal injection pressures on the 6 cracks.

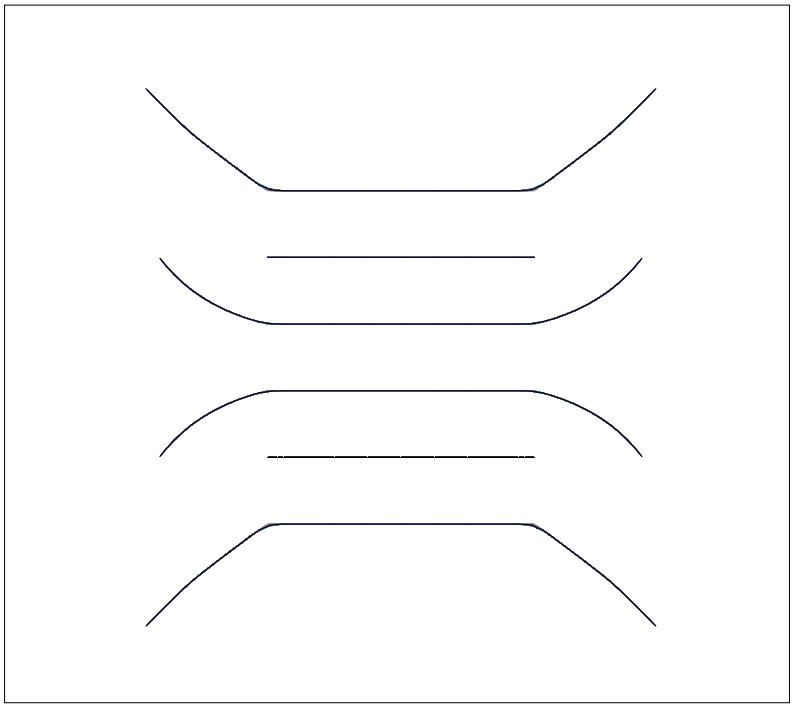

Figure 3.20: Six aligned cracks initially with $\frac{d}{a} = 0.5$, $\frac{h}{a} = 1$ and $a = 2$ grow into this configuration on application of equal injection volumes on the 6 cracks.

Chapter 4

Conclusions

This report presented a computational procedure utilizing a symmetric Galerkin boundary element method (SGBEM), based on a weakly singular, weak-form traction integral equation to model fractures in isotropic linearly elastic media. We assumed a crack geometry typical of hydraulic fracturing wherein the crack profile in the out-of-plane direction is expressed in terms of crack height. We then established that such cracks grow faster than pure 2D cracks when crack-crack interaction is important and crack height is comparable to crack length. The current version of the HyFrac2D code has several limitations. The constant internal pressure corresponding to an inviscid fluid inside the crack is a very simple model for hydraulic fracturing. Towards improving the model's response to fluid flow in the crack, the next major step would be to model fluid in the crack using finite elements. This would utilize a coupled SGBEM-FEM formulation that has already be derived and implemented for three dimensions, and could be reduced to two dimensions for implementation in HyFrac2D.

There is also a simplification in the way that the code calculates $\bar{K}_I$ and equates it to K_{IC}. We defined the equivalent mode-I SIF to be

$$\bar{K}_I = K_I \cos^3\left(\frac{\theta_g}{2}\right) - \frac{3}{2} K_{II} \cos\left(\frac{\theta_g}{2}\right) \sin\theta_g,$$

with the growth direction given by

$$\tan\left(\frac{\theta_g}{2}\right) = \frac{K_I - \sqrt{K_I^2 + 8K_{II}^2}}{4K_{II}}, \qquad -\pi \leq \theta_g \leq \pi$$

and the SIF's at crack tip m given by

$$K_m = K_m^0 + K_{mj}^P \alpha_j^P.$$

Thus we can write the growth angle in terms of the SIF's due to the remote stress and the pressures in each crack as

$$\tan\left(\frac{\theta_g}{2}\right) = \frac{1}{4}\left[\frac{K_I^0 + K_I^j \alpha_j}{K_{II}^0 + K_{II}^j \alpha_j} - \sqrt{8 + \left(\frac{K_I^0 + K_I^j \alpha_j}{K_{II}^0 + K_{II}^j \alpha_j}\right)^2}\right].$$

The presence of the remote stress SIF's mean that the growth angle is not a linear function of the SIF's and thus we do not know the growth angle until we compute the pressure scaling values. This means $\bar{K}_I$ cannot be computed a priori for each crack tip, nor can they be compared to K_{IC} to calculate the pressure scaling values and thus cannot be used to compute the amount that each tip will grow.

To get around this complication, we instead set $K_I = K_{IC}$ for the crack tip with the largest mode-I SIF, and scale the other cracks according to the

ratio of their mode-I SIF to K_{IC}. Let us consider two crack tips, with larger SIF's at the first crack tip such that the first crack tip will grow more than the second. For the first crack tip, we have

$$\frac{\bar{K}_I^{(1)}}{\bar{K}_{\max}} = \frac{\bar{K}_I^{(1)}}{\bar{K}_I^{(1)}} = \frac{K_I^{(1)}}{K_{IC}} = 1$$

and thus the crack tip growth the maximum amount whether we set K_I or $\bar{K}_I$ equal to K_{IC}. However for the second crack tip, we have

$$\frac{\bar{K}_I^{(2)}}{\bar{K}_{\max}} = \frac{\bar{K}_I^{(2)}}{\bar{K}_I^{(1)}} \neq \frac{K_I^{(2)}}{K_{IC}}$$

and therefore other crack tips do not grow the same amount with our simplification as they should in the real formulation. Additionally, the growth angles for all the cracks will not be identical in both formulations. The question is how much does this affect the crack growth behavior? When there is no remote stress, the two strategies are identical. Thus when the remote stress is small relative to the stresses produced by the pressures in crack, the effect on the crack growth behavior should also be small. It is thus left as an area of possible future work to correctly equate the equivalent mode-I stress intensity factor to the critical SIF.

References

1. Rungamornrat, J. (2004). *A Computational Procedure for Analysis of Fractures in Three-dimensional Anisotropic Media.* Ph.D. Thesis, The University of Texas at Austin.

2. Tran, H. D. (2010). *A Computational Procedure for Analysis of Fractures in Two-dimensional Multi-field Media.* Ph.D. Thesis, The University of Texas at Austin.

3. Murakami, Y. (Ed.) (1987). *Stress Intensity Factor Handbook*, Volume I. Oxford: Pergamon Press.

4. Erickson, A.J (2012). *Simulation of growth of multiple interacting 2D cracks in hydraulic fractures driven by inviscid fluid.* M.S.E. Report, The University of Texas at Austin.

Vita

Saumik Dana was born in Surat, Gujarat, India. He entered graduate school at The University of Texas at Austin in Fall 2012 at the Department of Aerospace Engineering and Engineering Mechanics. Prior to this, he graduated from the Indian Institute of Science, Bangalore in July 2011 with a Master of Engineering degree in Mechanical Engineering.

Email address: saumik@utexas.edu

This report was typeset with LaTeX[†] by the author.

[†]LaTeX is a document preparation system developed by Leslie Lamport as a special version of Donald Knuth's TeX Program.